



1 **Re-examining the 4.2 ka BP event in foraminifer isotope records from the Indus River delta**
2 **in the Arabian Sea**

3
4 Alena Giesche¹, Michael Staubwasser², Cameron A. Petrie³, and David A. Hodell¹

5
6 ¹ *Godwin Laboratory for Palaeoclimate Research, Department of Earth Sciences, University of*
7 *Cambridge, Cambridge, CB2 3EQ, United Kingdom*

8 ² *Institute for Geology und Mineralogy, University of Cologne, Zùlpicher Str. 49a, 50674 Cologne,*
9 *Germany*

10 ³ *Department of Archaeology, University of Cambridge, Cambridge, CB2 3DZ, United Kingdom*

11
12 *Correspondence to: Alena Giesche (ag927@cam.ac.uk)*

13
14
15
16
17
18
19
20
21
22
23
24
25
26
27
28
29
30
31
32
33
34
35
36
37
38
39
40
41
42
43
44
45
46
47
48
49
50
51



52 **Abstract**

53

54 The plains of northwest South Asia receive rainfall during both the Indian Summer (June-September)
55 and Winter (December-March) Monsoon. Researchers have long attempted to deconstruct the
56 influence of both precipitation regimes in paleoclimate records, in order to better understand regional
57 climatic drivers and their potential impact on human populations. The Mid-Late Holocene transition
58 between 5.3-3.3 ka BP is of particular interest in this region because it spans the period of the Indus
59 Civilization from its early development to eventual transformation. The oxygen isotope record of the
60 surface-dwelling planktonic foraminifer *Globigerinoides ruber* from the northeast Arabian Sea
61 provided evidence for an abrupt decrease in rainfall and reduction in Indus River discharge at 4.2 ka
62 BP, which the authors linked to the decline of the urban phase of the Indus Civilization (Staubwasser
63 et al., 2003). Given the importance of this study, we used the same core (63KA) to replicate the oxygen
64 isotope profiles of a larger size fraction of *G. ruber* than measured previously and, in addition, we
65 measured two other foraminifer species at decadal resolution over the interval from 5.4 to 3.0 ka BP.
66 By selecting both thermocline-dwelling (*Neogloboquadrina dutertrei*) and shallow-dwelling
67 (*Globigerinoides sacculifer*) species, we provide enhanced detail of the climatic changes that occurred
68 over this crucial time interval. We found evidence for a period of increased surface water mixing,
69 which we suggest was related to a strengthened winter monsoon with a peak intensity over 200 years
70 from 4.5 to 4.3 ka BP. The time of greatest change occurred at 4.1 ka BP when both the summer and
71 winter monsoon weakened, resulting in a reduction in rainfall in the Indus region. The earliest phase
72 of the Mature Harappan period coincided with the period of inferred stronger winter monsoon
73 between 4.5-4.3 ka BP, whereas the end of the urbanized phase followed the decrease in both the
74 summer and winter monsoon strength by 4.1 ka BP. Our findings provide evidence that the initial
75 growth of large Indus urban centers was coincident with increased winter rainfall, whereas the
76 contraction of urbanism and change in subsistence strategies followed a reduction in rainfall of both
77 seasons.

78

79

80

81

82

83

84

85

86

87

88

89

90

91

92

93

94

95

96

97

98

99

100

101 **1. Introduction**

102

103 The ~4.2 ka BP event is considered to be a defining event of the Mid-Late Holocene transition
104 period (Mayewski et al., 2004), and is marked by intense aridity in much of western Asia,
105 which has been linked to cultural transitions in Mesopotamia, Egypt, and the Indus Civilization
106 (Staubwasser and Weiss, 2006; Weiss, 2016). Recently, a climate reconstruction from
107 Mawmluh cave in northeastern India has been used to formally demarcate the post-4.2 ka BP
108 time as the Meghalayan Age (Letter from the 44th International Union of Geological Sciences,
109 2018; Walker et al., 2012). However, defining the exact timing and extent of aridity at ~4.2 ka
110 BP remains an open question (Finné et al., 2011; Wanner et al., 2008). In this special issue
111 devoted to the “4.2 ka event”, we provide new paleoclimate data from a marine core in the
112 northern Arabian Sea over this critical time interval to better understand the changes that
113 occurred in hydroclimate over the Indian Subcontinent.

114

115 The $\delta^{18}\text{O}$ record of *Globigerinoides ruber* from marine core 63KA, obtained from the Arabian
116 Sea off the coast of Pakistan and produced by Staubwasser et al. (2003), was among the first
117 well-resolved paleoclimate records to suggest a link between a decrease in Indus River
118 discharge around 4.2 ka BP and the decline of the Indus Civilization. Since the publication of
119 this record, several other terrestrial paleoclimate reconstructions from the region
120 (Berkelhammer et al., 2012; Dixit et al., 2014, 2018; Giosan et al., 2012; Kathayat et al., 2017;
121 Menzel et al., 2014; Nakamura et al., 2016; Prasad and Enzel, 2006), and a number of marine
122 reconstructions (Giosan et al., 2018, in review; Gupta et al., 2003; Ponton et al., 2012) have
123 added to our understanding of the complex relationship between the Indus Civilization and
124 climate change. New questions have also emerged about the relative importance of winter
125 rain from the Indian Winter Monsoon (IWM) system and summer rain from the Indian
126 Summer Monsoon (ISM) during the critical time period from 5.4 to 3.0 ka BP, which spans the
127 pre-urban, urban, and post-urban phases of the Indus Civilization (Giosan et al., 2018, in
128 review; Petrie et al., 2017; Prasad and Enzel, 2006).

129

130 At its height, the Indus Civilization spanned a considerable geographical area with a greater
131 extent than all the other ancient civilizations of its time (Agrawal, 2007; Possehl, 2003;
132 Wheeler, 1968). Today, the region that was once occupied by Indus populations is marked by
133 a heterogeneous rainfall pattern, and some sites in the central Thar desert receive as little as
134 100 mm yr⁻¹, which is only about 10% of the amount of direct annual rainfall seen in the
135 northeastern region close to New Delhi. Scarce direct precipitation in the central regions
136 around the Thar Desert is supplemented in some cases by fluvial or groundwater sources. In
137 addition, the distribution of winter rain (increasing towards the northwest) is distinct from
138 summer rain (increasing towards the east), making regions variably suitable for growing
139 certain crops and grazing (Petrie et al., 2017; Petrie and Bates, 2017). While many
140 paleoclimate studies from South Asia have theorized about the overall climatic impact of
141 drought (and in most cases identified summer monsoon as the cause), it is important to
142 identify changes in the relative contributions and timing of seasonal rainfall from both the
143 winter and summer monsoons. Previously, it has not been possible to reliably differentiate
144 winter and summer rain in reconstructions from the Indus region.

145

146 In this study, we re-examined the same marine core (63KA) used in the original Staubwasser
147 et al. (2003) paper. We first assessed the reproducibility of the *Globigerinoides ruber* $\delta^{18}\text{O}$



148 record using a larger size fraction of the same species for the time period 5.4-3.0 ka BP. We
149 also measured the $\delta^{18}\text{O}$ of two additional foraminifer species, *G. sacculifer* (*Globigerinoides*
150 *sacculifer*) and *N. dutertrei* (*Neogloboquadrina dutertrei*), which live deeper than *G. ruber* in
151 the water column. The different ecologies of these two species provide additional information
152 with which to evaluate the multiple $\delta^{18}\text{O}$ records and assess seasonal changes in the
153 paleoceanography of the northeastern Arabian Sea near the mouth of the Indus River.

154
155 The $\delta^{18}\text{O}$ of foraminifera has been widely applied as an indicator of temperature and salinity
156 changes (Duplessy et al., 1992; Maslin et al., 1995; Wang et al., 1995; Rohling, 2000).
157 Measuring the $\delta^{18}\text{O}$ of species calcifying at different depths can provide further information
158 about upper ocean seasonal hydrography such as surface water mixing, depth of the
159 thermocline, and upwelling (Ravelo and Shackleton, 1995). Such methods have been applied
160 by several other studies (Billups et al., 1999; Cannariato and Ravelo, 1997; Norris, 1998;
161 Steinke et al., 2010; Steph et al., 2009; among others), including a reconstruction of East Asian
162 Winter Monsoon strength in the South China Sea (Tian et al., 2005). We applied a similar
163 method to samples from core 63KA in the northeastern Arabian Sea because surface waters
164 at this location are influenced by freshwater discharge from the Indus River and direct
165 precipitation during the summer monsoon months, whereas enhanced upper ocean mixing
166 and upwelling occur during the winter monsoon. By comparing the $\delta^{18}\text{O}$ of multiple species
167 of foraminifera we seek to infer variations in the relative strengths of the summer and winter
168 monsoons, and by comparing the 63KA record to other nearby marine and terrestrial records
169 we evaluate the potential role that climate played in cultural transformation of the Indus
170 Civilization.

171 172 **2. Site Description**

173 174 *2.1 Monsoon – land-based processes*

175
176 Today, most of the annual precipitation over northwest South Asia stems from the ISM, and
177 occurs mainly between June and September. The pressure gradient between the low-
178 pressure Tibetan Plateau and high-pressure Indian Ocean is accompanied by the ITCZ
179 (Intertropical Convergence Zone) reaching its northward maximum in summer, which draws
180 in moisture over the subcontinent via southwesterly winds from the Indian Ocean (Fleitmann
181 et al., 2007; Gadgil, 2003). The summer rainfall gradient increases from the central Thar
182 Desert (as little as 100 mm direct summer rainfall per year) to the Himalaya mountains in the
183 north (>1000 mm) and the Aravalli range to the west (>500 mm) (Figure 1b).

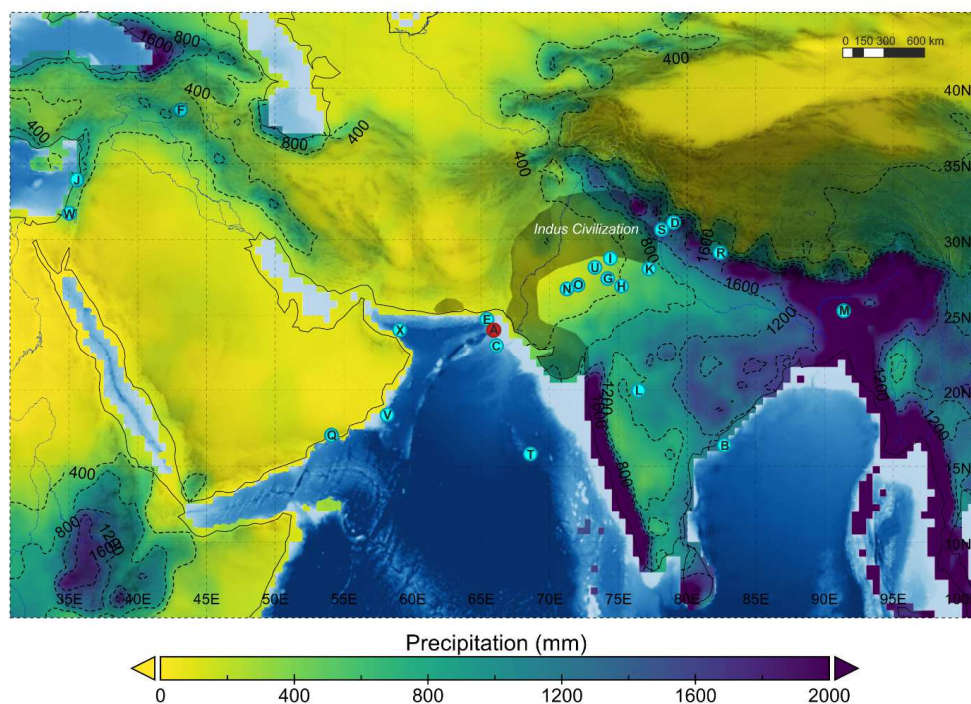
184
185 The IWM rain falls between December through March, and is mainly the result of atmospheric
186 Western Disturbances (Dimri and Dash, 2012; Yadav et al., 2012) originating over the
187 Mediterranean and Black Sea (Hatwar et al., 2005) that allow for moisture incursion from the
188 Arabian Sea (Rangachary and Bandyopadhyay, 1987). During the IWM, the pressure gradient
189 is reversed from the summer condition, allowing the passage of Western Disturbances when
190 the ITCZ moves southward. As winter transitions to spring, predominantly northeasterly
191 winds shift to westerly winds (Sirocko, 1991) that result in peak winter rainfall over the plains
192 of northwest India in February and March. The winter rainfall gradient increases from the
193 southern Thar Desert (<10 mm per year) up to the Himalayas in the northwest (>400 mm)



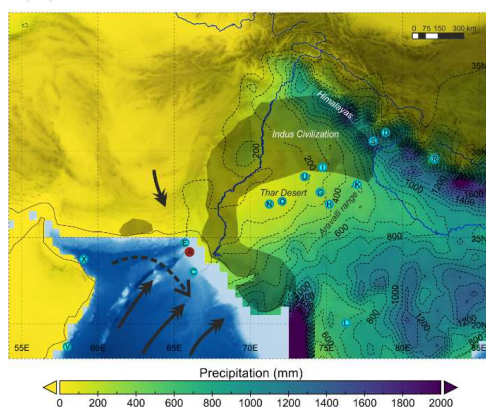
194 (Figure 1c). Overall, the IWM contributes between roughly 10 to 50% of the total annual
 195 rainfall of northwest South Asia today.

196

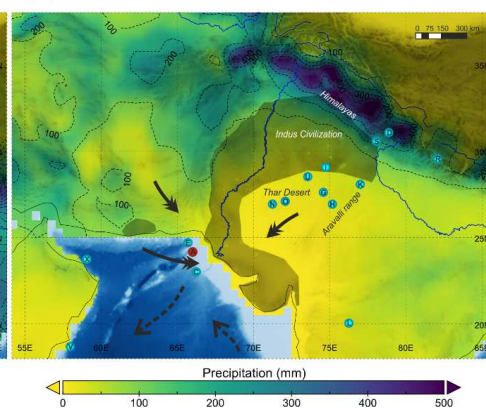
(a) Longterm mean (1981-2011) annual precipitation



(b) Longterm mean (1981-2011) summer precipitation



(c) Longterm mean (1981-2011) winter precipitation



197

198 **Figure 1. a. Annual b. ISM (JJAS) c. IWM (DJFM) mean precipitation (1981-2011) isohyets taken from**
 199 **the GPCC V7 global gridded dataset (0.5° x 0.5° resolution); note the difference in scale for summer**
 200 **and winter precipitation (0-2000 mm vs. 0-500 mm). Rainfall data overlain on GEBCO 2014 ocean**
 201 **bathymetry dataset, and shaded region shows extent of the Indus Civilization. Bold arrows show main**
 202 **wind directions, dashed arrows show ocean surface currents. Other studies discussed in this paper**
 203 **indicated by letters:**



204

- A Core 63KA – (this study; Staubwasser et al., 2003) M Mawmluh cave speleothem – (Berkelhammer et al., 2012)
- B Core 16A – (Ponton et al., 2012)
- C Core Indus 11C – (Giosan et al., 2018, in review) N Kanod playa lake – (Deotare et al., 2004)
- D Din Gad peat record – (Phadtare, 2000) O Bap Malar playa lake – (Deotare et al., 2004)
- E Core 39KG and 56KA – (Doose-Rolinski et al., 2001) Q Qunf cave speleothem – (Fleitmann et al., 2003)
- F Lake Van record – (Wick et al., 2003; Lemcke and R Rara lake – (Nakamura et al., 2016)
- Sturm, 1997) S Sahiya cave speleothem – (Kathayat et al., 2017)
- G Didwana playa lake – (Singh et al., 1990) T Foraminifer trap EAST – (Curry et al., 1992)
- H Sambhar playa lake – (Sinha et al., 2006) U Lunkaransar playa lake – (Enzel et al., 1999)
- I Karsandi playa lake – (Dixit et al., 2018) V Core 723A, RC27-14, RC27-23, RC27-28 – (Gupta et al., 2003), (Overpeck et al., 1996)
- J Jeita cave speleothem – (Cheng et al., 2015)
- K Kotla Dahar lake – (Dixit et al., 2014) W Soreq cave speleothem – (Bar-Matthews et al., 2003; Bar-Matthews and Ayalon, 2011)
- L Lonar lake – (Menzel et al., 2014) X Core M5-422 – (Cullen et al., 2000)

205

206 The Indus and the other rivers that make up Punjab are partly fed by winter snow and ice melt
207 from their upper mountain catchment areas. Melting peaks during the summer months
208 around July-August (Yu et al., 2013), which coincides with the peak of ISM rainfall, and Indus
209 River discharge reaches its maximum during August (Karim et al., 2002). The proportion of
210 winter to summer precipitation contributing to the Indus River is not entirely clear, although
211 one study has estimated a 64-72% contribution of winter precipitation from the deuterium
212 excess of Indus River water (Karim et al., 2002), whereas a previous study estimated a lower
213 15-44% contribution of snowmelt to Indus tributaries (Ramasastri, 1999). Since the 1960s, the
214 Indus River has seen a more than a 50% reduction in discharge because of the construction
215 of barrages as well as the diversion of water for agricultural uses (Ahmad et al., 2001).

216

217 *2.2 Hydrography – ocean-based processes*

218

219 Core 63KA was obtained by the PAKOMIN cruise in 1993 (von Rad et al., 1995). The laminated
220 core from the northeastern Arabian Sea (24° 37' N, 65° 59' E) was taken at 316 m water depth
221 on the continental shelf, ~100 km west of the Indus River delta. The core has high
222 sedimentation rates (equivalent to a temporal resolution of around 18 years/cm in the period
223 of interest, 5.4-3.0 ka BP), and all foraminifer proxies were produced from the same laminated
224 core with no bioturbation. An important aspect of core 63KA is that different components of
225 the monsoon system are co-registered in the same sediment core, thereby permitting an
226 explicit evaluation of the relative timing of different parts of the climate system (e.g., ISM and
227 IWM). Modern hydrographic conditions in the northeastern Arabian Sea are highly influenced
228 by the seasonal monsoon. During summertime, highest sea surface temperatures (SSTs) are
229 observed along with a shallow mixed layer depth <25 m (Schulz et al., 2002) (Figure 2a). A low
230 salinity plume surrounds the Indus River delta and shoreline extending as far as the coring
231 location (Supplemental Figure S1). The reverse occurs in winter when the lowest SSTs are
232 accompanied by surface water mixing to >125 m, resulting in warming of the deeper waters
233 (Schulz et al., 2002). During the transition from winter to spring, wind directions shift from
234 northeasterly to westerly (Sirocko, 1991), promoting a period of upwelling in the
235 northeastern Arabian Sea (Staubwasser et al., 2002; Rao, 1981).

236

237 The northern Arabian Sea is dominated by highly saline (up to 37 psu) surface waters of the
238 Arabian Sea High Salinity Water Mass (ASHSW), which extend from the surface up to 100 m
239 depth (Joseph and Freeland, 2005). This high salinity can be explained by the high evaporative

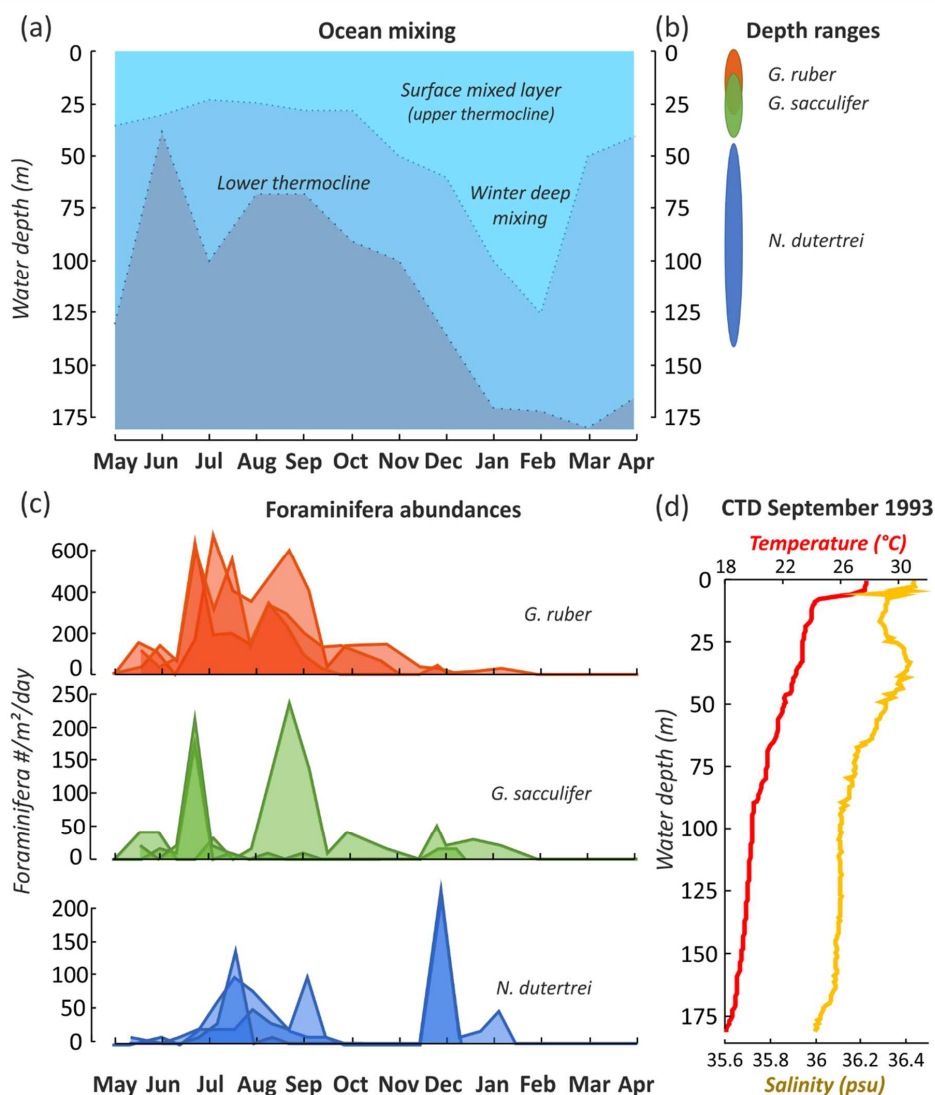


240 rates over this region. Along coastal areas the ASHSW is starkly contrasted by the fresh water
241 discharge of the Indus River, combined with direct precipitation. In contrast, surface waters
242 in the Bay of Bengal on the eastern side of India have much lower surface water salinity,
243 because of overall higher precipitation and stronger stratification from weaker winds (Shenoi
244 et al., 2002). The heightened evaporative conditions and highly saline surface waters of the
245 northeastern Arabian Sea make it a sensitive study location to observe changes in discharge
246 of the entire Indus River catchment area – ultimately tracking changes in monsoon strength.
247 Unlike individual terrestrial records, which may be affected by local climatic processes, the
248 marine record from core 63KA is more likely to integrate regional changes of the large-scale
249 ocean-atmosphere system.

250

251 Planktonic foraminifera complete their life cycle within a few weeks (Bé and Hutson, 1977).
252 Peak abundances indicate the time of year when each species tends to calcify, thereby
253 recording the $\delta^{18}\text{O}$ of the seawater in their CaCO_3 shells primarily during certain seasons.
254 Foraminifer abundances in the eastern Arabian Sea have been studied by Curry et al. (1992)
255 using sediment traps deployed at shallow (~1400 m) and deep (~2800 m) water depths (“T”
256 in Figure 1a). Peak abundances for *G. ruber* and *G. sacculifer* occur during the summer months
257 (June-September), whereas *N. dutertrei* peak mainly during the winter as well as with a
258 secondary peak in summer months (Figure 2c). Preferred depth ranges for each species reflect
259 their ecological niches, including requirements for nutrients and tolerance for ranges of
260 temperature and salinity (Bé and Hutson, 1977; Hemleben et al., 2012). *G. ruber* lives in the
261 upper surface waters (0-10 m), *G. sacculifer* is found in slightly deeper surface waters (10-40
262 m), and *N. dutertrei* inhabits the base of the mixed layer near the thermocline (40-140 m)
263 (estimates based on ranges from Farmer et al. (2007) and the local CTD profile) (Figure 2d).

264



265
 266 **Figure 2.** a. Seasonal surface water mixing depth based on station EPT-2 located nearby the coring site
 267 of 63KA (adapted from Schulz et al., 2002 who also used data from Hastenrath and Lamb, 1979) b.
 268 Foraminifera depth ranges based on CTD profile c. Foraminifera abundances from EAST trap: *G. ruber*
 269 (orange), *G. sacculifer* (green), and *N. dutertrei* (blue) (adapted from Curry et al., 1992 using Zaric,
 270 2005) d. CTD temperature (red) and salinity (yellow) profile from station 11 at coring location, taken
 271 September 1993 (von Rad, 2013).

272

273 3. Materials and Methods

274

275 3.1 Age model

276

277 The radiocarbon dates from Staubwasser et al. (2002, 2003) were obtained from 80 samples
 278 of mainly the foraminifera *G. sacculifer* and three samples of *O. universa*. In the interval of



279 interest (5.4-3.0 ka BP), there are 15 radiocarbon dates with a 95% confidence range of 30-
280 130 years. Bayesian age modelling software, BACON v2.3.3 (Blaauw and Christen, 2011), was
281 used as an R-package to update the age model of core 63KA (Supplemental Figure S5, Table
282 S2). IntCal13 was used for radiocarbon calibration (Reimer et al., 2013) with marine reservoir
283 ages provided by Staubwasser et al. (2002, 2003).

284

285 3.2 Stable isotope analysis

286

287 Oxygen and carbon isotopes were measured on three species of foraminifera selected from
288 washed samples at 1-cm intervals throughout the core: *G. ruber* (white, *sensu stricto*), *G.*
289 *sacculifer*, and *N. dutertrei*. For *G. ruber*, 12 ± 8 foraminifera were picked from the 400-500µm
290 size fraction with an average weight of 21.4 ± 2.5µg. The 400-500µm size fraction was picked
291 because too few specimens remained in the size fraction 315-400µm used by Staubwasser et
292 al. (2003). For *G. sacculifer*, 34 ± 7 foraminifera were picked from the 315-400µm size fraction
293 with an average weight of 21.9 ± 2.6µg. For *N. dutertrei*, 34 ± 4 foraminifera were picked from
294 the 315-400µm size fraction with an average weight of 25.9 ± 2.2µg. At some depth levels in
295 the core there were insufficient foraminifera for measurement, leaving 11 gaps in the *G. ruber*
296 400-500µm record, 3 gaps in the *G. sacculifer* record, and no gaps for *N. dutertrei*. The
297 published *G. ruber* is from the 315-400µm size fraction and contains 17 gaps in the depth
298 range examined (Staubwasser et al., 2003).

299

300 All foraminifera were weighed, crushed, and dried at 50° C. Samples were cleaned for 30
301 minutes with 3% H₂O₂, followed by a few drops of acetone, ultrasonication, and drying
302 overnight. Where sample weights exceeded 80µg, oxygen and carbon isotopes were
303 measured using a Micromass Multicarb Sample Preparation System attached to a VG SIRA
304 Mass Spectrometer. In cases of smaller sample sizes, the Thermo Scientific Kiel device
305 attached to a Thermo Scientific MAT253 Mass Spectrometer was used in dual inlet mode. This
306 method adds 100% H₃PO₄ to the CaCO₃, water is removed cryogenically, and the dry CO₂ is
307 analyzed isotopically by comparison with a laboratory reference gas. For both measurement
308 methods, 10 reference carbonates and 2 control samples were included with every 30
309 samples. Results are reported relative to VPDB, and internal precision is better than ±0.08‰
310 for δ¹⁸O and ±0.06‰ for δ¹³C. External precisions were estimated by five triplicate (three
311 separately picked) measurements of *G. ruber* (400-500µm) that yielded one standard
312 deviation of ±0.12‰ (δ¹⁸O) and ±0.10‰ (δ¹³C). For *G. sacculifer* (315-400µm) the standard
313 deviation of eight triplicate measurements were ±0.07‰ (δ¹⁸O) and ±0.07‰ (δ¹³C), and for
314 *N. dutertrei* (315-400µm) the standard deviation of nine triplicate measurements was
315 ±0.06‰ (δ¹⁸O) and ±0.07‰ (δ¹³C).

316

317 To calculate equilibrium values of δ¹⁸O_{calcite(PDB)}, we used the CTD profile from station 11
318 (24.62° N, 66.07° E) (Figure 2d) taken during PAKOMIN *Sonne* cruise no. 90 (von Rad, 2013),
319 which is nearly identical to the location of core 63KA (24.62° N 65.98° E). The δ¹⁸O_{water(SMOW)}
320 was calculated from salinity following Dahl and Oppo (2006), and δ¹⁸O_{calcite(SMOW)} was further
321 calculated using the calcite-water equation of Kim and O'Neil (1997). We also used the
322 equation of Shackleton (1974) as a comparative method for calculating δ¹⁸O_{calcite(PDB)}.

323

324 3.3 Statistical treatment

325



326 As in the original data of Staubwasser et al. (2003), the oxygen isotope results show great
327 variability and distinguishing long-term trends in these data requires statistical smoothing. To
328 reduce the variance in the data and identify trends, the $\delta^{18}\text{O}$ and $\delta^{13}\text{C}$ data from 5.4-3.0 ka BP
329 were first resampled to constant 1-year intervals using linear interpolation. A loess (locally
330 weighted) smoothing function was then applied to the data, using a 210-year moving window
331 as described by Staubwasser et al. (2003). Loess smoothing uses weighted least squares,
332 which places more importance on the data points closest to the center of the smoothing
333 interval. The bandwidth of 210 years was considered an optimal time window for capturing
334 the overall trends in the dataset (other time windows are shown for comparison in
335 Supplemental Figure S2).

336

337 Statistical tests were applied to the $\delta^{18}\text{O}$ and $\delta^{13}\text{C}$ time series, including the package SiZer
338 (Sonderegger et al., 2009) in R software (2016) that calculates whether the derivative of a
339 time series exhibits significant changes given a range of timespans. We applied a range of
340 smoothing windows (bandwidth of 20-500 years) to assess the significance of changes in the
341 isotope records throughout the time series. Where step changes occur in $\delta^{18}\text{O}$ we also
342 conducted a Student's t-test to determine if the mean population of $\delta^{18}\text{O}$ is significantly
343 different before and after the change.

344

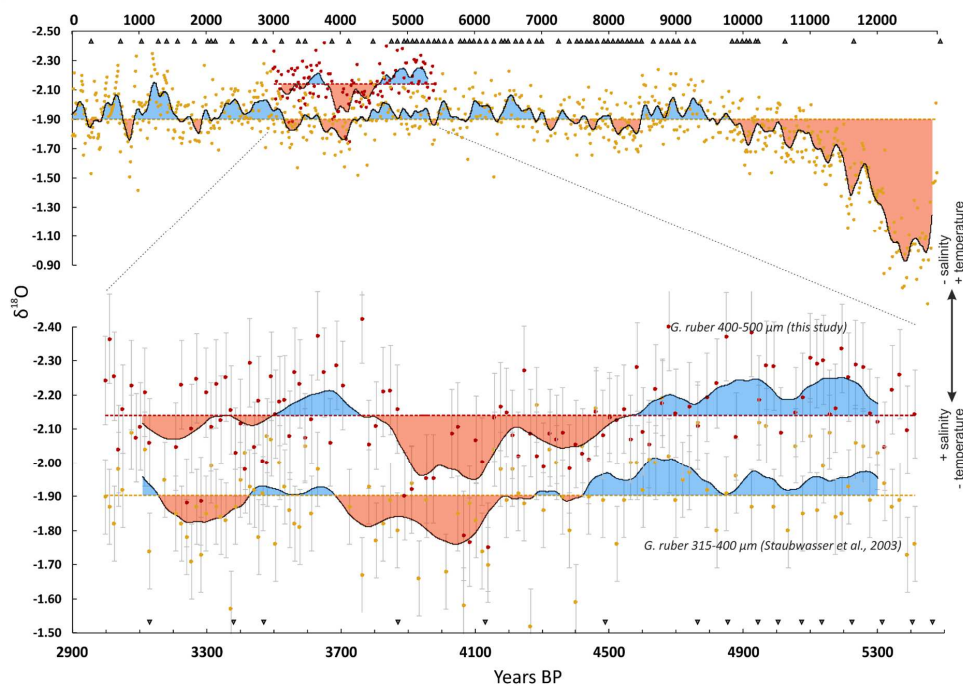
345 4. Results

346

347 The new $\delta^{18}\text{O}$ measurements of *G. ruber* (400-500 μm) parallel the published record of *G.*
348 *ruber* (315-400 μm) (Staubwasser et al., 2003), but the $\delta^{18}\text{O}$ of the specimens from the larger
349 size fraction is offset by -0.23‰ on average (Figure 3). The two records, produced in different
350 laboratories by different investigators, display a weak correlation for the raw data ($R = 0.2$,
351 slope 0.27, intercept -1.33) and a strong correlation for the 210-year smoothed records ($R =$
352 0.7 , slope 0.53, intercept -0.77). When comparing the two *G. ruber* records, it is apparent that
353 the increasing trend in $\delta^{18}\text{O}$ starts well before ~ 4.2 ka BP – perhaps as early as ~ 4.9 ka BP. This
354 trend is also observed with the SiZer analysis, which identifies a significant increase in $\delta^{18}\text{O}$
355 anywhere from 4.9 to 4.2 ka BP depending on which smoothing window is selected (Figure
356 4). The new $\delta^{18}\text{O}$ record of *G. ruber* (400-500 μm) shows additional detail after the ~ 4.2 ka BP
357 event – i.e. specifically, a double-peak maximum occurring at 4.1 and 3.95 ka BP that is
358 related to seven discrete measurements with high $\delta^{18}\text{O}$ values. These maxima are offset from
359 the average $\delta^{18}\text{O}$ value by +0.18‰ (smoothed average), or up to +0.38‰ when considering
360 the maximum individual measurement at 4.1 ka BP. The offsets from the average values
361 exceed one standard deviation of the entire record from 5.4-3.0 ka BP, which is 0.13‰. A
362 Student's t-test comparing the means of pre- and post-4.1 ka BP indicates that the +0.07‰
363 shift in mean $\delta^{18}\text{O}$ values of *G. ruber* (315-400 μm) is statistically significant (t value = 2.9, $p <$
364 0.01), and the +0.04‰ shift in mean $\delta^{18}\text{O}$ values of *G. ruber* (400-500 μm) is weakly significant
365 (t value = 1.7, $p < 0.1$).

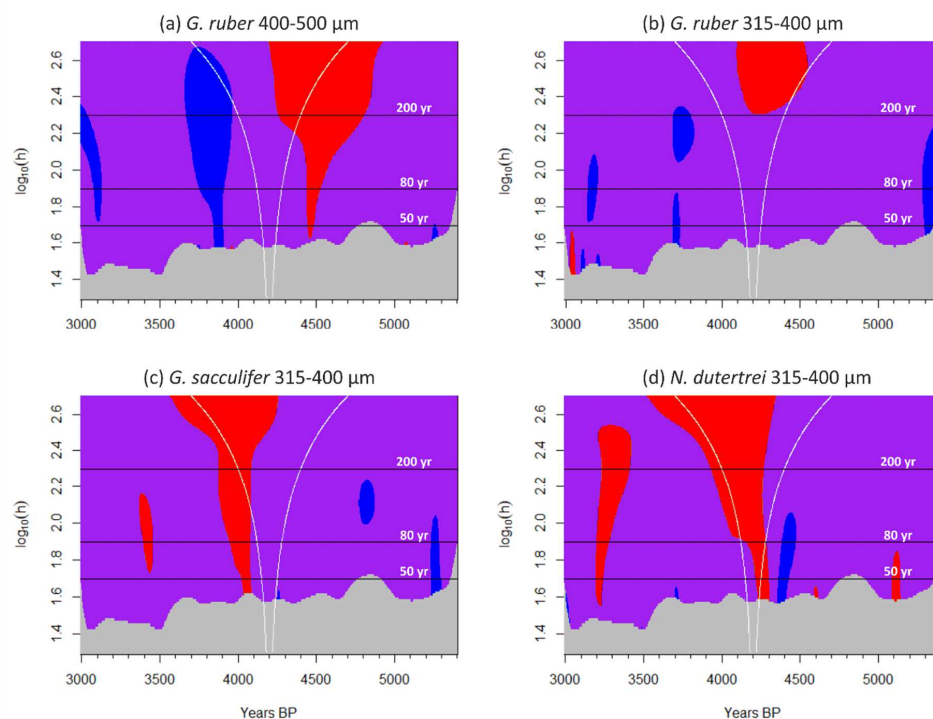
366

367



368
369
370
371
372
373

Figure 3. Core 63KA $\delta^{18}O$ *G. ruber* from two size fractions: 400-500 μm (red) (this study), 315-400 μm (orange) (Staubwasser et al., 2003), shown zoomed in over 5.4-3.0 ka BP. Data shown with a 210-year loess smoothing and $\pm 1\sigma$ error bars. Individual AMS radiocarbon dates are denoted by triangles near the timeline.



374

375

376

377

378

379

380

381

382

383

384

385

386

387

388

389

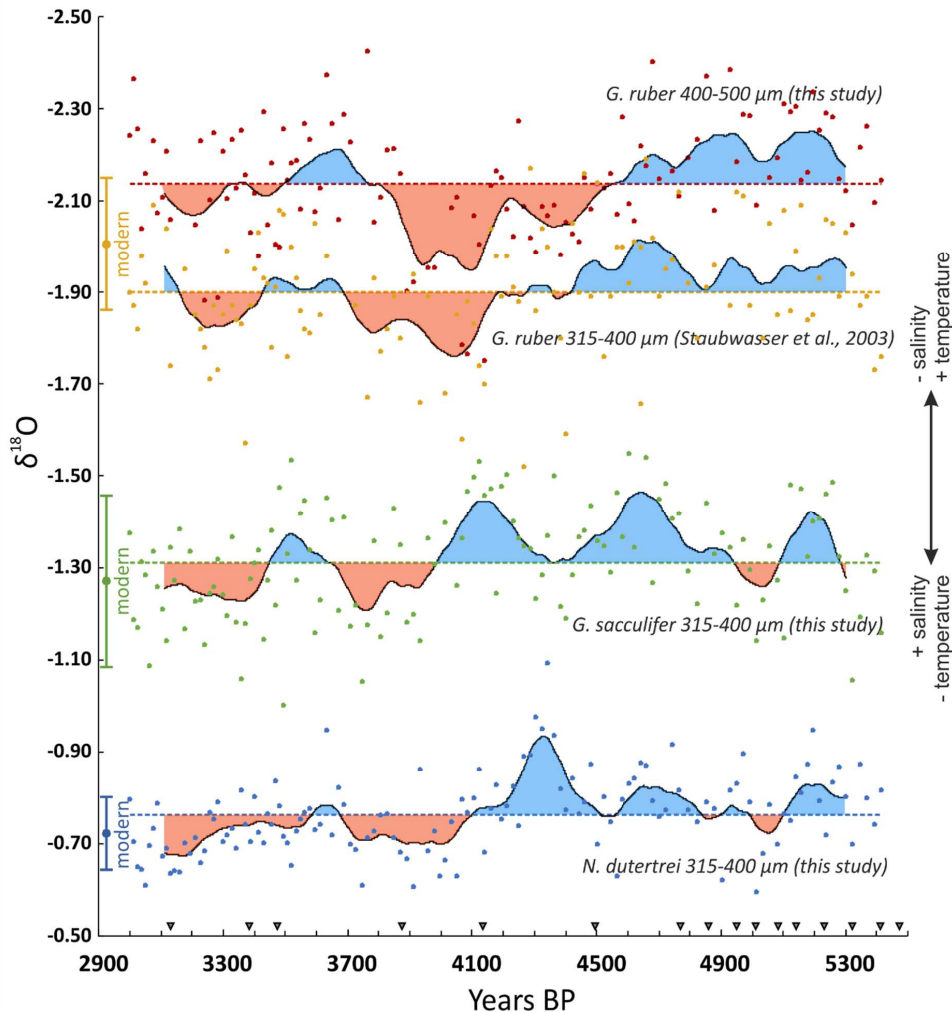
390

391

392

Figure 4. SiZer 1st derivative analysis (Sonderegger et al., 2009) applied to $\delta^{18}\text{O}$ of **a.** *G. ruber* 400-500 μm , **b.** *G. ruber* 315-400 μm , **c.** *G. sacculifer* 315-400 μm , **d.** *N. dutertrei* 315-400 μm . Statistically significant increases (red) and decreases (blue) are shown alongside times with no significant change (purple). The smoothing bandwidth (h) ranges from 20 to 500 years (denoted by the width between the white lines), and three bandwidths have been highlighted by black horizontal lines at h = 50, 80, and 200 years.

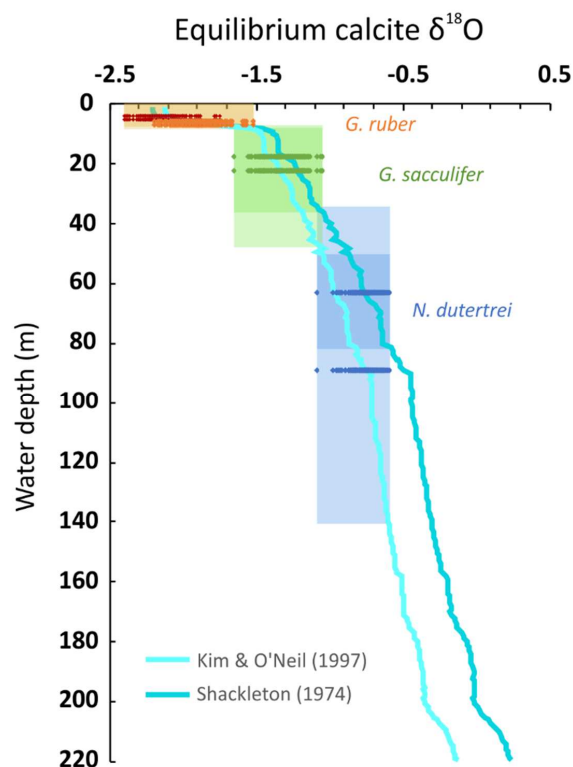
The relative differences in $\delta^{18}\text{O}$ of the planktonic species studied (*G. ruber*, *G. sacculifer* and *N. dutertrei*) reflect the temperature and salinity of their habitat in the water column: $\delta^{18}\text{O}$ *G. ruber* < $\delta^{18}\text{O}$ *G. sacculifer* < $\delta^{18}\text{O}$ *N. dutertrei* (Figure 5). *G. sacculifer* is offset from *G. ruber* (315-400 μm) by approximately +0.57‰, whereas *N. dutertrei* is offset by +1.14‰. The larger size fraction of *G. ruber* (400-500 μm) is offset from *G. ruber* (315-400 μm) by -0.23‰. The offsets among species are maintained throughout the entire record (Figure 5). We also measured $\delta^{18}\text{O}$ values near the top of the core (approximately the last 200 years) for all three species in the 315-400 μm size fraction, which continue to show the same offsets (Supplemental Figure S3). The $\delta^{18}\text{O}$ of *G. ruber* shows the greatest variance and *N. dutertrei* shows the least (Supplemental Figure S4, Table S1).



393
394 **Figure 5.** Core 63KA $\delta^{18}\text{O}$ *G. ruber* from two size fractions: 400-500 μm (red) (this study), 315-400 μm
395 (orange) (Staubwasser et al., 2003), *G. sacculifer* 315-400 μm (this study), and *N. dutertrei* 315-400 μm
396 (this study). Data shown with a 210-year loess smoothing, modern surface values $\pm 1\sigma$ shown for
397 comparison. Individual AMS radiocarbon dates are denoted by triangles near the timeline.

398
399 Equilibrium calcite calculations based on the salinity and temperature measurements from
400 the September 1993 CTD profile of station 11 of the PAKOMIN Cruise (von Rad, 2013) show
401 the expected depth habitats of the three foraminifer species (Figure 6). *G. ruber* is generally
402 found at 0-30 m, *G. sacculifer* at 15-40 m, and *N. dutertrei* at 60-150 m (Farmer et al., 2007).
403 Using the CTD profile from our core location, we compare these depth ranges with the
404 measured $\delta^{18}\text{O}$ values. The calculated depths ranges agree well with those expected on the
405 basis of other studies, placing *G. ruber* in the upper 10 m, *G. sacculifer* 10-40 m, and
406 *N. dutertrei* 40-140 m.

407

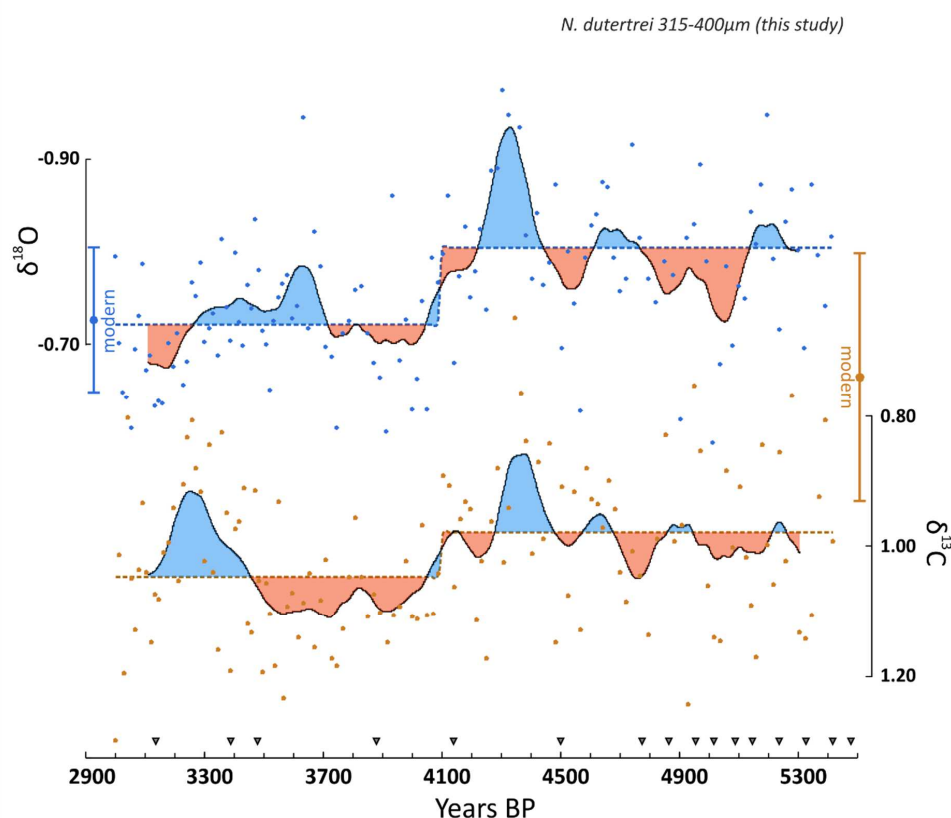


408
409 **Figure 6.** $\delta^{18}\text{O}$ of equilibrium calcite calculated from CTD profile at station 11 (von Rad, 2013) with
410 projected depth ranges of *G. ruber* 400-500 μm (red), *G. ruber* 315-400 μm (orange), *G. sacculifer* 315-
411 400 μm (green), *N. dutertrei* 315-400 μm (blue). We show estimated values using both the original
412 paleotemperature equation of Shackleton (1974) (dark teal), and Kim & O'Neil (1997) (turquoise).
413 Horizontal ranges show the measured $\delta^{18}\text{O}$ values of each species between 5.4-3.0 ka BP.

414
415 The most obvious trend in the *G. sacculifer* $\delta^{18}\text{O}$ is the increase around 4.1 ka BP. A Student's
416 t-test comparing the means of pre- and post-4.1 ka BP indicates that the +0.07‰ shift in mean
417 $\delta^{18}\text{O}$ values is statistically significant (t value = 3.9, $p < 0.01$). SiZer analysis also points to a
418 statistically significant increase at ~4.1-3.9 ka BP, when considering all smoothing time
419 windows between 20 and 500 years (Figure 4).

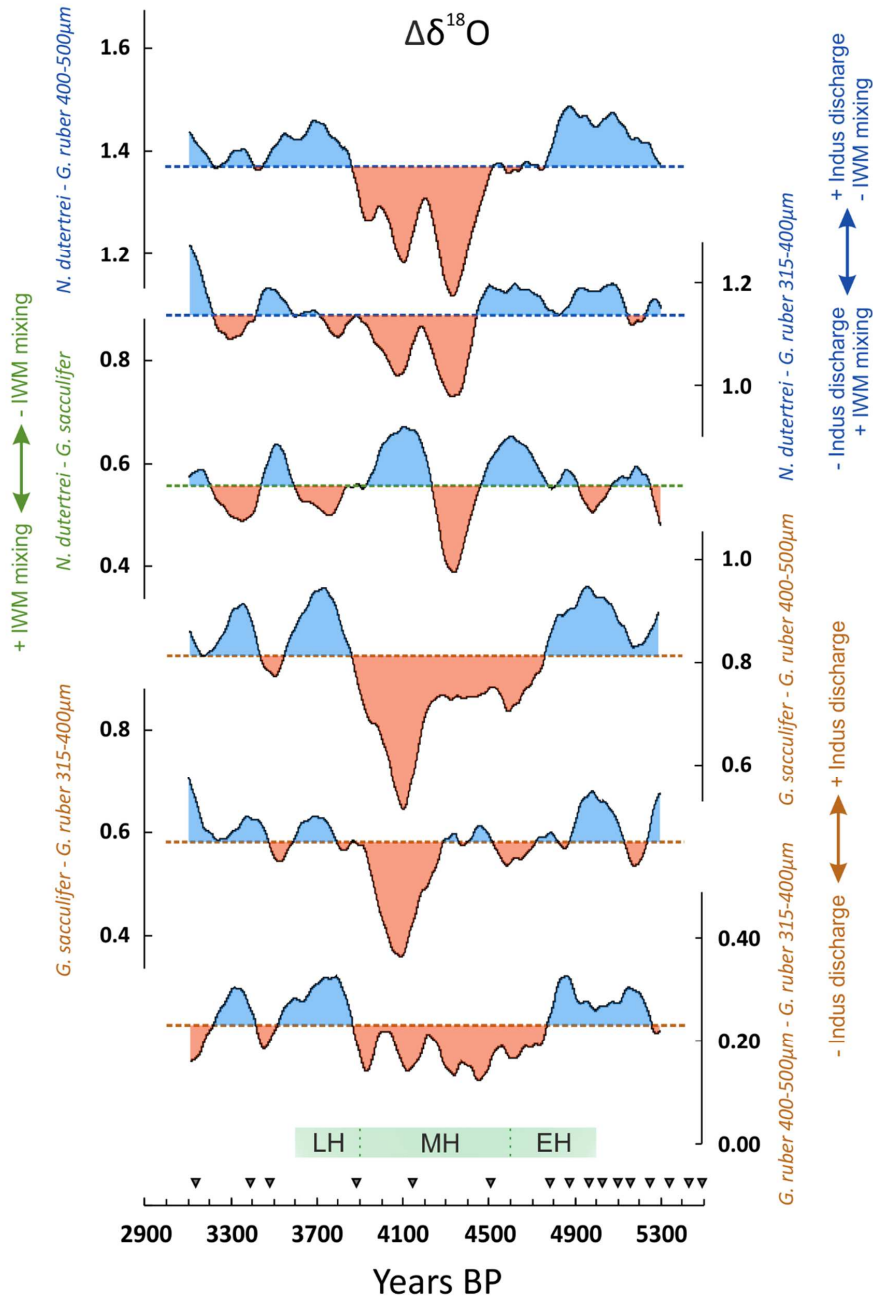
420
421 The dominant trend in the $\delta^{18}\text{O}$ of *N. dutertrei* is a mean increase at 4.1 ka BP (Figure 7). SiZer
422 analysis also identifies a significant decrease in $\delta^{18}\text{O}$ occurring mainly between 4.45 and 4.35
423 ka BP, followed by a significant increase between 4.3 and 4.1 ka BP (Figure 4). A Student's t-
424 test comparing the means of pre- and post-4.1 ka BP indicates that the +0.08‰ shift in mean
425 $\delta^{18}\text{O}$ values is statistically significant (t value = 6.3, $p < 0.01$).

426



427
 428 **Figure 7.** Core 63KA $\delta^{18}\text{O}$ (top) and $\delta^{13}\text{C}$ (bottom) of *N. dutertrei* 315-400 μm . Data shown with a 210-
 429 year loess smoothing, modern surface values $\pm 1\sigma$ shown for comparison. Individual AMS radiocarbon
 430 dates are denoted by triangles near the timeline.

431
 432 Differencing $\delta^{18}\text{O}$ of foraminifera (expressed as $\Delta^{18}\text{O}$) in the same sample can sometimes
 433 improve the signal-to-noise ratio (Figure 8). The $\Delta^{18}\text{O}$ of *G. ruber* 400-500 μm and *G. ruber*
 434 315-400 μm size fractions shows increasing similarity between ~ 4.8 and 3.9 ka BP during the
 435 period of overall higher $\delta^{18}\text{O}$. The $\Delta^{18}\text{O}$ of *N. dutertrei* and both size fractions of *G. ruber*,
 436 designated $\Delta\delta^{18}\text{O}_{d-r}$, reveals a period of more similar values between ~ 4.5 and 3.9 ka BP, with
 437 two minima at 4.3 and 4.1 ka BP. The $\Delta^{18}\text{O}$ of *G. sacculifer* and both size fractions of *G. ruber*
 438 ($\Delta\delta^{18}\text{O}_{s-r}$), shows a period of similar values between 4.3 and 3.9 ka BP, with a minimum
 439 difference at 4.1 ka BP. In contrast, the $\Delta^{18}\text{O}$ of *N. dutertrei* and *G. sacculifer* ($\Delta\delta^{18}\text{O}_{d-s}$), shows
 440 the most similarity between 4.5 and 4.2 ka BP with a minimum at 4.3 ka BP, followed by the
 441 maximum differences between 4.2 and 3.9 ka BP that peaks at 4.1 ka BP.
 442



443
 444 **Figure 8.** Core 63KA $\Delta\delta^{18}\text{O}$. Data shown with a 210-year loess smoothing. Individual AMS radiocarbon
 445 dates are denoted by triangles near the timeline. *G. ruber* 315-400 μm size fraction data from
 446 Staubwasser et al. (2003). The green band near the timeline showing EH, MH, and LH refers to Early
 447 Harappan (~5.0-4.6 ka BP), Mature Harappan (~4.6-3.9 ka BP), and Late Harappan (~3.9-3.6 ka BP),
 448 respectively.
 449



450 5. Discussion

451

452 5.1 Interpretation of foraminifer $\delta^{18}\text{O}$

453

454 The original $\delta^{18}\text{O}$ record of *G. ruber* (315-400 μm) by Staubwasser et al. (2003) is confirmed
455 by our independent $\delta^{18}\text{O}$ measurements of *G. ruber* in a larger size fraction (400-500 μm). The
456 larger size fraction is offset by approximately -0.2‰, which is similar to the size-related
457 fractionation of -0.3‰ per +100 μm for *G. ruber* reported by Cayre and Bassinot (1998), and
458 could be attributed to size-related vital effects. Alternatively, the offset might be explained
459 by interlaboratory calibration considering the data were produced using two different
460 methods and mass spectrometers.

461

462 The observed 4.1 ka BP maximum in $\delta^{18}\text{O}$ of *G. ruber*, living near the surface during summer
463 months, could be attributed to either decreased SST or increased surface water salinity
464 (Bemis et al., 1998). Staubwasser et al. (2003) acknowledged that a decrease in SST could
465 cause the increase in $\delta^{18}\text{O}$ in the *G. ruber* record, but argued that this explanation is unlikely
466 because a *G. ruber* $\delta^{18}\text{O}$ record from core M5-422 in the northwestern Arabian Sea shows
467 opposing trends over the same time period (Cullen et al., 2000), and a local alkenone SST
468 proxy record shows relatively higher temperatures in the same period (Dooze-Rolinski et al.,
469 2001). If the ~0.2‰ (relative to mean) increase in $\delta^{18}\text{O}$ of *G. ruber* at 4.1 ka BP was caused by
470 temperature change rather than salinity, a ~1° C cooling of surface water is implied (Kim and
471 O'Neil, 1997).

472

473 Following Staubwasser et al. (2003), we interpret the $\delta^{18}\text{O}$ variations of *G. ruber* to be
474 predominantly a salinity signal. Salinity at the core site is dependent on changes in Indus River
475 discharge, local run-off, and direct precipitation. Although the ISM would be the main
476 influence on direct precipitation and run-off at the coring location, changes in the IWM could
477 also influence Indus River discharge, because snowmelt is a significant contributor in the
478 upper Indus catchment (Karim et al., 2002) and peaks during the summer months (Yu et al.,
479 2013).

480

481 The thermocline-dwelling foraminifera *N. dutertrei* shows maximum abundances during
482 winter, and are interpreted to reflect winter mixing. Weaker IWM winds are expected to
483 result in a shorter duration and/or less intense upper ocean mixing, although how this signal
484 is ultimately related to the amount or distribution of winter rainfall in the Indus River
485 catchment has not been demonstrated conclusively. Dimri (2006) studied Western
486 Disturbances for the time period 1958-1997, and noted that surplus years of winter
487 precipitation are linked to significant heat loss over the northern Arabian Sea, which is mainly
488 attributed to intensified westerly moisture flow and enhanced evaporation. Such conditions
489 would promote deeper winter mixing, and provide a basis for relating thermocline depth with
490 IWM intensity. During weak IWM conditions, colder unmixed water would result in higher
491 $\delta^{18}\text{O}$ values of *N. dutertrei*, whereas enhanced mixing and homogenization of the water
492 column under strong IWM conditions would decrease $\delta^{18}\text{O}$. The minimum of $\delta^{18}\text{O}$ in *N.*
493 *dutertrei* occurs between 4.5 and 4.3 ka BP, pointing to a period of strengthened IWM. We
494 interpret the stepped increase in $\delta^{18}\text{O}$ of *N. dutertrei* at 4.1 ka BP to represent a decrease in
495 IWM wind-driven mixing. Similarly, $\delta^{13}\text{C}$ of *N. dutertrei* increases significantly after 4.1 ka BP
496 (Figure 7), which would also suggest reduced upwelling of low $\delta^{13}\text{C}$ intermediate water under



497 a weaker IWM (Lynch-Stieglitz, 2006). According to the $\delta^{18}\text{O}$ signal of *N. dutertrei*, the
498 temperature pattern in the thermocline implies surface cooling between 4.5 and 4.3 ka BP
499 and surface warming after 4.1 ka BP interrupted only by a period of cooling between 3.7 and
500 3.3 ka BP, which is in broad agreement with records of alkenone sea-surface temperature
501 estimates from cores in the northeastern Arabian Sea ("E" in Figure 1) (Dooze-Rolinski et al.,
502 2001; Staubwasser, 2012).

503

504 5.2 Interpretation of foraminifer $\Delta^{18}\text{O}$

505

506 By using $\Delta\delta^{18}\text{O}$ between foraminifer species, we can distinguish additional processes affecting
507 the surface waters and thermocline (Ravelo and Shackleton, 1995). This technique has been
508 used previously to infer changes in the strength of the East Asian Winter Monsoon (EAWM)
509 in the South China Sea (Tian et al., 2005), as well as mixed layer and thermocline depth in
510 other studies (Billups et al., 1999; Cannariato and Ravelo, 1997; Norris, 1998). Here we use
511 the difference in the $\delta^{18}\text{O}$ of *G. ruber* and *N. dutertrei* ($\Delta\delta^{18}\text{O}_{d-r}$) to track changes in the
512 surface-to-deep gradient. This gradient can be driven by either $\delta^{18}\text{O}$ changes in the surface-
513 dwelling (*G. ruber*) and/or the thermocline-dwelling species (*N. dutertrei*). During times of a
514 strengthened winter monsoon, $\Delta\delta^{18}\text{O}_{d-r}$ will decrease as surface waters are homogenized and
515 the thermocline deepens. Similarly, $\Delta\delta^{18}\text{O}_{d-r}$ will also decrease during times of a weakened
516 summer monsoon, as decreased Indus River discharge will increase surface water salinity and
517 $\delta^{18}\text{O}$ of *G. ruber* will become more similar to *N. dutertrei*.

518

519 *G. sacculifer* is also a surface dweller, but has a slightly deeper depth habitat than *G. ruber*.
520 We thus expect *G. ruber* to be more influenced by surface salinity variations than *G. sacculifer*,
521 and suggest the $\delta^{18}\text{O}$ difference between the two species ($\Delta\delta^{18}\text{O}_{s-r}$), reflects the influence of
522 Indus River discharge on near surface salinity. The greatest difference in $\Delta\delta^{18}\text{O}_{s-r}$ occurs at 4.1
523 ka BP, which is interpreted as an increase in surface water salinity (Figure 8).

524

525 The difference in $\delta^{18}\text{O}$ between *G. sacculifer* and *N. dutertrei* ($\Delta\delta^{18}\text{O}_{d-s}$) also reflects surface
526 mixing and thermocline depth, but *G. sacculifer* is less affected by surface salinity changes
527 than *G. ruber*. Thus, the responses of $\Delta\delta^{18}\text{O}_{d-s}$ and $\Delta\delta^{18}\text{O}_{d-r}$ can be used to differentiate
528 between surface water salinity changes and wind-driven mixing. Accordingly, simultaneously
529 low $\Delta\delta^{18}\text{O}_{d-s}$ and $\Delta\delta^{18}\text{O}_{d-r}$ indicate a period of increased surface water mixing and increased
530 IWM (such as the period between 4.5 and 4.3 ka BP), but times of relatively low $\Delta\delta^{18}\text{O}_{d-s}$ but
531 high $\Delta\delta^{18}\text{O}_{d-r}$ and $\Delta\delta^{18}\text{O}_{s-r}$ (around 5.0 ka BP) indicate periods of increased Indus discharge and
532 strength of the ISM and IWM.

533

534 However, the following period of low $\Delta\delta^{18}\text{O}_{d-r}$ but high $\Delta\delta^{18}\text{O}_{d-s}$ from 4.1-3.9 ka BP is likely
535 driven by increased salinity of surface water. This distinction becomes clearer when
536 examining the $\Delta\delta^{18}\text{O}_{s-r}$, where increased similarity from 4.8-3.9 ka BP (with a sharp increase
537 at 4.1 ka BP) reflects the effect of increased sea surface salinity that reduces the $\delta^{18}\text{O}$
538 difference between *G. ruber* and *G. sacculifer*. At the same time, weakened winter mixing
539 increases $\Delta\delta^{18}\text{O}_{d-s}$, which occurs from 4.2-3.9 ka BP. Importantly, the proxies also indicate that
540 increased IWM mixing is generally positively correlated with increased Indus discharge, and
541 vice versa. The single time period when this does not hold true is 4.5-4.25 ka BP, when
542 increased IWM mixing is coupled with decreased Indus discharge.

543



544 In summary, our multi-species approach using $\delta^{18}\text{O}$ of *G. ruber*, *G. sacculifer*, and *N. dutertrei*
545 allows us to differentiate between strength of the IWM and freshwater discharge of the Indus
546 River. We suggest that ISM strength decreased gradually from at least 4.8 ka BP, while the
547 IWM strength peaked around 4.5-4.3 ka BP and then weakened afterwards. It is unlikely that
548 the abrupt increase in *G. ruber* $\delta^{18}\text{O}$ at 4.1 ka BP and low $\Delta\delta^{18}\text{O}_{s-r}$ could be caused solely by
549 the decrease in IWM strength, even though IWM contributes to Indus River discharge.
550 Weakening of the ISM must have played a substantial role in the 4.1 ka BP shift as well,
551 indicated by the period 4.5-4.25 ka BP, when Indus discharge reflected a weak ISM ($\Delta\delta^{18}\text{O}_{s-r}$)
552 despite a phase of strengthened IWM.

553

554 5.3 Comparison to marine records

555

556 The interpretation of core 63KA relies on proxies that directly link surface water salinity to
557 ISM precipitation and Indus River discharge, and thermocline shifts to related IWM-driven
558 mixing. Additionally, there is an established mechanism relating mixing with IWM strength,
559 as anomalously cool and evaporative conditions over the northern Arabian Sea (promoting
560 deeper winter mixing) correlates with increased winter precipitation in the western
561 Himalayas (Dimri, 2006). The strength of the 63KA core lies in its highly resolved age model,
562 high sedimentation rates and its position in particularly saline surface waters (ASHSW) close
563 to highly contrasting freshwater sources. Additionally, both the ISM and IWM are co-
564 registered in proxies in the same laminated core with no bioturbation, thereby permitting an
565 explicit evaluation of the relative timing of the two monsoons.

566

567 Other marine records from the Arabian Sea also suggest a gradual decrease in ISM strength
568 since ~5 ka BP (Gupta et al., 2003; Overpeck et al., 1996). Cullen et al. (2000) observed an
569 abrupt peak in aeolian dolomite and calcite in marine sediments in the Gulf of Oman from
570 4.0-3.6 ka BP, and Ponton et al. (2012) also showed a shift to weaker ISM after 4.0 ka BP in
571 the Bay of Bengal, based on $\delta^{13}\text{C}$ of leaf waxes. Marine IWM reconstructions are not
572 particularly coherent: although Dooze-Rolinski et al. (2001) find a decrease in evaporation
573 and weakening of the ISM between 4.6 and 3.7 ka BP, they argue this was accompanied by a
574 relative increase in IWM strength. Giosan et al. (2018, in review) inferred enhanced winter
575 monsoon conditions from 4.5-3.0 ka BP based on a planktic paleo-DNA and % *Globigerina*
576 *falconensis* record close to our coring site ("C" in Figure 1), which contradicts our finding of
577 decreased upper ocean mixing after 4.3 ka BP. We suggest the chronological resolution of
578 core 63KA paired with a multi-species foraminifer $\delta^{18}\text{O}$ record can provide more detail about
579 the timing of changes in IWM and ISM strength.

580

581 5.4 Comparison to regional terrestrial records

582

583 The 63KA $\delta^{18}\text{O}$ record obtained from three foraminifer species highlights several important
584 ocean-atmosphere changes over the 5.4-3.0 ka BP time period. First, a sharp decrease
585 occurred in both summer and winter precipitation at 4.1 ka BP, which is within a broader 300-
586 year period of increased aridity spanning both rainfall seasons between 4.2 and 3.9 ka BP. In
587 detail, we infer a relative decrease in Indus River discharge and weakened ISM between 4.8
588 and 3.9 ka BP, peaking at 4.1 ka BP, while a 200-year phase of strong IWM interrupted this
589 period from 4.5-4.3 ka BP. Furthermore, the stepped change in $\delta^{18}\text{O}$ of *N. dutertrei* suggests
an enduring change in ocean-atmosphere conditions after 4.1 ka BP.



591

592 A relatively abrupt ~4.2 ka BP climate event has been observed in several terrestrial records
593 on the Indian subcontinent, most notably Mawmluh Cave (~4.1-3.9 ka BP) in northeastern
594 India (Berkelhammer et al., 2012) and Kotla Dahar (~4.1 ka BP) in northwestern India (Dixit et
595 al., 2014) (Figure 9). A less abrupt yet still arid period is documented in a peat profile (~4.0-
596 3.5 ka BP) from northcentral India (Phadtare, 2000), at Lonar Lake (~4.6-3.9 ka BP) in central
597 India (Menzel et al., 2014), and at Rara Lake (~4.2-3.7 ka BP) in western Nepal (Nakamura et
598 al., 2016). Finally, a recent study of oxygen and hydrogen isotopes in gypsum hydration water
599 from Karsandi on the northern margin of the Thar Desert showed wet conditions between 5.1
600 and 4.4 ka BP, after which the playa lake dried out sometime between 4.4 and 3.2 ka BP (Dixit
601 et al., 2018). Considering terrestrial records can record more local climatic conditions than
602 marine records, it is remarkable that the records collectively agree on a regional phase of
603 aridity between 4.2 and 3.9 ka BP within the uncertainties of the age models that vary
604 considerably among records.

605

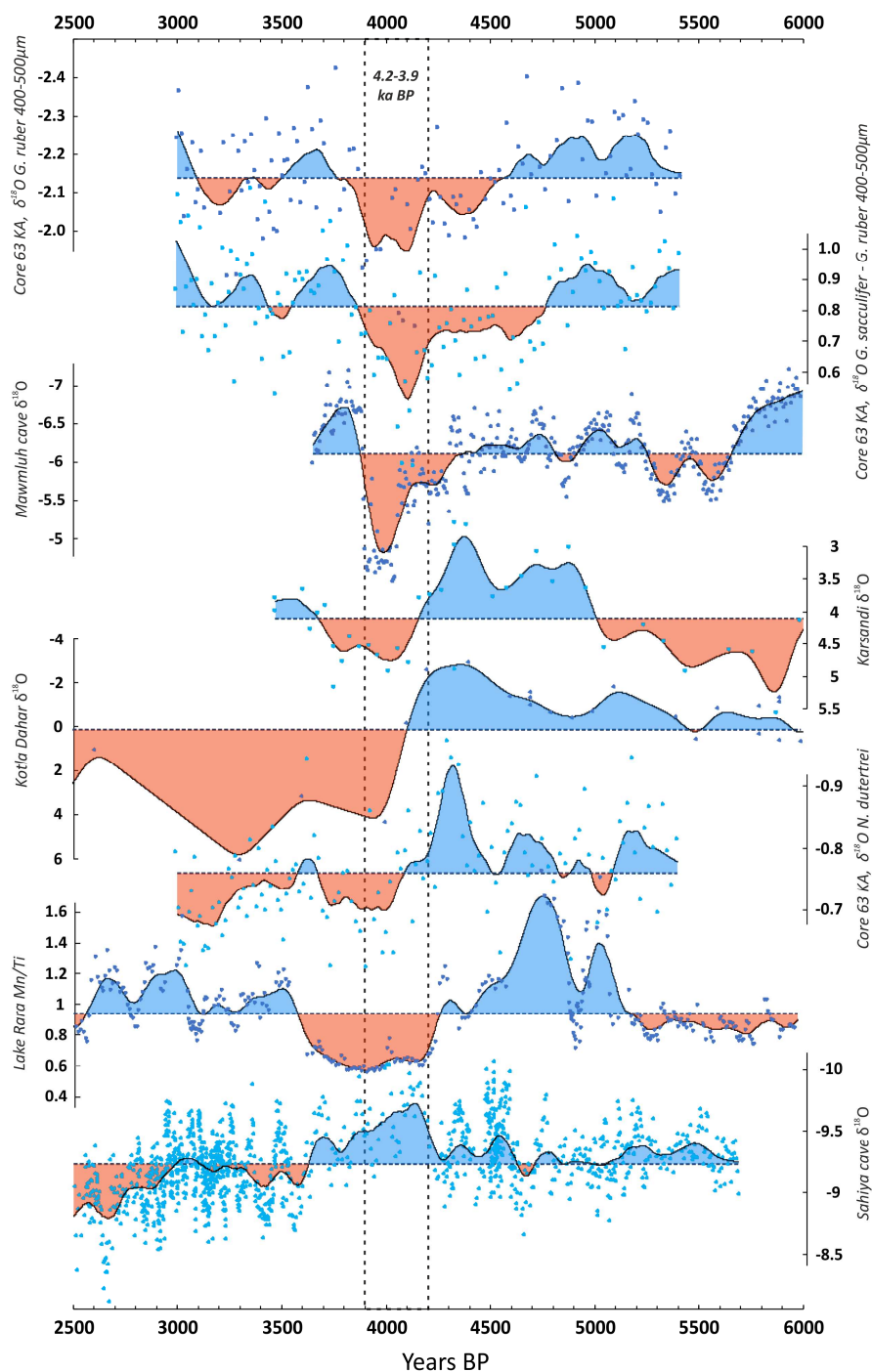
606 However, not all records support this finding, such as a reconstruction from Sahiya Cave in
607 northwestern India that shows an abrupt decrease in $\delta^{18}\text{O}$ interpreted to reflect an increase
608 in monsoon strength from ~4.3-4.15 ka BP, followed by an arid trend after 4.15 ka BP
609 (Kathayat et al., 2017). In addition, several other Thar Desert records do not identify a “4.2 ka
610 BP event” *sensu stricto*, but instead suggest that lakes dried out several centuries earlier
611 (Deotare et al., 2004; Enzel et al., 1999; Singh et al., 1990) or later (Sinha et al., 2006) than 4.2
612 ka BP. This discrepancy may relate to non-linear climate responses of lakes, which would not
613 record a drought at 4.2 ka BP if they had already dried out earlier from the ongoing decrease
614 in summer rainfall. In addition, there are also significant concerns about chronological
615 uncertainties when using radiocarbon of bulk sediment for dating in some of these records.
616 It is also possible that variations in the timing of climate change inferred from the terrestrial
617 records may be real, reflecting different sensitivity to ISM and IWM rain. As a marine record,
618 core 63KA integrates large-scale ocean-atmosphere changes, and therefore can help inform
619 the interpretation of the more locally sensitive terrestrial records.

620

621 More distantly, several terrestrial records in the Middle East also show a decrease in winter
622 precipitation proxies around 4.2 ka BP: Jeita Cave in Lebanon records a relatively dry period
623 between 4.4 and 3.9 ka BP (Cheng et al., 2015) and Soreq Cave in Israel shows a period of
624 increased aridity starting at ~4.3 ka BP (Bar-Matthews et al., 2003; Bar-Matthews and Ayalon,
625 2011) (Figure 10). Lake Van in eastern Turkey also records reduced spring rainfall and
626 enhanced aridity after ~4.0 ka BP (Wick et al., 2003; Lemcke and Sturm, 1997). All records
627 suggest a relatively arid phase in winter precipitation after ~4.3 ka BP, as inferred from core
628 63 KA. Qunf Cave in Oman (Fleitmann et al., 2003), which is outside the range of IWM
629 influence, instead shows a steady mid-Holocene weakening of the ISM that closely follows
630 trends in summer solar insolation. Core 63 KA also infers a protracted decrease in ISM since
631 ~4.8 ka BP.

632

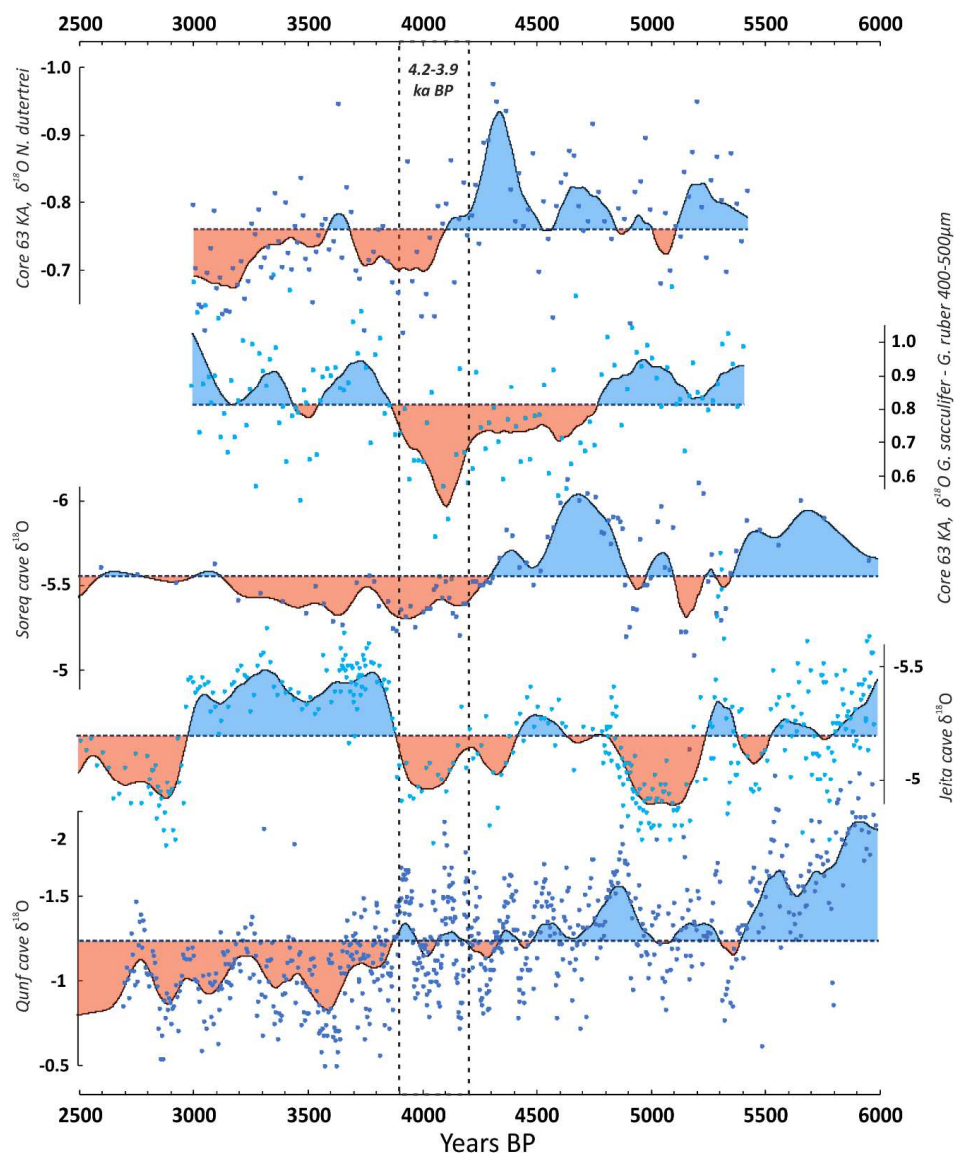
633



634
 635 **Figure 9.** Comparison of the $\delta^{18}\text{O}$ record of core 63KA with terrestrial records from the Indian
 636 Subcontinent, from top to bottom: this study (first two), Berkelhammer et al., 2012; Dixit et al., 2018;
 637 Dixit et al., 2014; this study; Nakamura et al., 2016; Kathayat et al., 2017.



638



639
 640 **Figure 10.** Comparison of the $\delta^{18}\text{O}$ record of core 63KA (topmost records) with more distant records,
 641 from top to bottom: Bar-Matthews et al., 2003; Cheng et al., 2015; and Fleitmann et al., 2003. Mean
 642 value for each record is taken for all available data between 6.0-2.5 ka BP.

643

644 *5.5 Cultural impacts*

645

646 Based on our reconstruction of reduced IWM mixing after 4.3 ka BP, accompanied by
 647 decreased freshwater discharge of the Indus River, it is worth considering what impacts could
 648 be expected from a reduction in IWM and ISM precipitation. A weakened IWM overlying a



649 reduced or more variable ISM would likely result in a distinct climate signal over the Indus
650 River catchment, with broad implications for seasonal river flow and water availability
651 throughout the year. The presence of the two rainfall systems creates a complex and diverse
652 range of ecologies across northwest South Asia (Petrie et al., 2017). In a situation when rainfall
653 in both seasons is reduced over extended periods, step-shifts in the natural environment may
654 occur that are difficult to reverse (desertification, lake desiccation, regional vegetation
655 changes, decline in overbank flooding and shift in river avulsion patterns).

656
657 Societies reliant on IWM, ISM, or a combination of the two would have been vulnerable to
658 years with monsoon failure, and a shift affecting both seasons will have challenged resilience
659 and tested sustainability (Green and Bates et al. in prep.; Petrie et al., 2017). Archaeological
660 research into the transition from the urban Mature Harappan phase (~4.6-3.9 ka BP) to the
661 post-urban Late Harappan phase (~3.9-3.6 ka BP) notes progressive deurbanization through
662 the abandonment of large Indus cities and a depopulation of the most western Indus regions,
663 concurrent with a general trend towards an increase of concentrations of rural settlements
664 in some areas of the eastern Indus extent (Green and Petrie, 2018; Petrie et al., 2017; Possehl,
665 1997) (Figure S6). The relatively limited range of well-resolved available archaeobotanical
666 data suggests that there was a degree of diversity in crop choice and farming strategies in
667 different parts of the Indus Civilization across this time span (Petrie et al., 2016; Petrie and
668 Bates, 2017; Weber, 1999; Weber et al., 2010). Farmers in southerly regions appear to have
669 focused on summer or winter crops, while the more northern regions of Pakistan Punjab and
670 Indian Punjab and Haryana were capable of supporting combinations of winter and summer
671 crops (Petrie and Bates, 2017). Although there is evidence for diverse cropping practices
672 involving both summer and winter crops in the northern areas during the urban period,
673 agricultural strategies appear to favor more drought-resistant summer crops in the Late
674 Harappan period (Madella and Fuller, 2006; Petrie and Bates, 2017; Pokharia et al., 2017;
675 Weber, 2003; Wright, 2010). It has previously been suggested that weakened ISM was a major
676 factor in these shifts (e.g. Giosan et al., 2012; Madella and Fuller, 2006). On the basis of our
677 reconstruction of decreased IWM in northwest South Asia after 4.3 ka BP with a step-shift at
678 4.1 ka BP, we suggest that both IWM and ISM climatic factors played a role in the
679 redistribution of population to smaller settlements in eastern regions with more direct
680 summer rain, as well as the observed shift to more summer crop dominated cropping
681 strategies.

682

683 **6. Conclusion**

684

685 This study expanded on the $\delta^{18}\text{O}$ record of planktonic foraminifer in core 63KA of the
686 northeastern Arabian Sea, originally published by Staubwasser et al. (2003). Using $\delta^{18}\text{O}$ of the
687 surface-dwelling foraminifera *G. ruber*, the original study inferred an abrupt reduction in
688 Indus River discharge at ~4.2 ka BP. Our further $\delta^{18}\text{O}$ analysis of a larger size fraction of this
689 species confirmed maximum salinity at 4.1 and 3.95 ka BP. In addition, the $\delta^{18}\text{O}$ difference
690 between the surface-dwelling *G. ruber* and slightly deeper-dwelling *G. sacculifer* ($\Delta\delta^{18}\text{O}_{s-r}$)
691 reveals that surface waters were more saline than average for the period from 4.8-3.9 ka BP.
692 By also measuring a thermocline-dwelling planktonic foraminiferal species, *N. dutertrei*, we
693 infer an increase in the strength of the IWM between 4.5 and 4.3 ka BP, followed by reduction
694 in IWM-driven mixing that peaks at 4.1 ka BP.

695



696 Assuming that weaker IWM mixing implies a reduction in IWM rainfall amount or duration
697 over northwest South Asia under past climatic conditions, the 63KA core is used to infer
698 important changes in seasonal hydrology of the Indus River catchment. We propose a
699 combined weakening of the IWM and ISM at 4.1 ka BP led to what has been termed the “4.2
700 ka BP” drought over northwest South Asia. The intersection of both a gradually weakening
701 ISM since 4.8 ka BP and a maximum decrease in IWM strength at 4.1 ka BP resulted in a
702 spatially layered and heterogeneous drought over a seasonal to annual timescale. Regions in
703 the western part of the Indus River basin accustomed to relying mainly on winter rainfall (also
704 via river run-off) would have been most severely affected by such changes. Regions in the
705 northeastern and eastern extents benefitted more from summer rainfall, and would have
706 been less severely affected, particularly as the ISM appears to recover strength by 3.9 ka BP.

707
708 Relatively strengthened IWM surface water mixing between 4.5 and 4.3 ka BP correlates with
709 a period of higher precipitation recorded at Karsandi on the northern margin of the Thar
710 Desert (Dixit et al., 2018), an area within the summer rainfall zone that is sensitive to small
711 changes in winter precipitation. This time span also represents the beginnings of the Mature
712 Harappan phase (Possehl, 2002; Wright, 2010), which implies that increasingly urbanized
713 settlements may have flourished under a strengthened IWM. With a weakening of the IWM
714 at ~4.1 ka, eastern regions with more access to ISM rainfall may have been more favorable
715 locations for agriculture. This may also help explain the broad shift in population towards
716 more rural settlements in the northeastern extent of the Indus Civilization that occurred by
717 ~3.9 ka BP (Possehl, 1997; Petrie et al., 2017), and a shift to more drought-tolerant kharif
718 (summer) season crops in Gujarat (Pokharia et al., 2017) and at Harappa (Madella and Fuller,
719 2006; Weber, 2003).

720
721 Given the importance of the relationships between humans and the environment during the
722 time of the Indus Civilization, understanding the impact of the IWM on precipitation
723 variability in northwest South Asia remains a critical area of research. We especially need a
724 better understanding of the wind patterns and moisture pathways that controlled the IWM
725 in the past. Disentangling both the length and intensity of seasonal precipitation is a crucial
726 aspect of understanding the impact of climate change on past societies, particularly in a
727 diverse region relying on mixed water sources (e.g., fluvial, ground aquifer, direct rainfall).

728

729 **Data availability**

730

731 Data presented in the paper can be accessed by contacting the corresponding author at
732 ag927@cam.ac.uk. After final acceptance of the manuscript, the data will also be uploaded
733 to an online database.

734

735 **Author contributions**

736

737 M.S. supplied core 63KA material, A.G. prepared the material for isotopic measurements, and
738 A.G. and D.A.H. interpreted the results. A.G., D.A.H., and C.A.P. wrote the manuscript.

739

740 **Competing interests**

741

742 The authors declare that they have no conflict of interest.



743

744 **Acknowledgements**

745

746 This work was supported by the ERC-funded TwoRains project. The authors thank the
747 following persons at the University of Cambridge: Maryline Vautravers for foraminifera
748 identification, James Rolfe and John Nicolson for $\delta^{18}\text{O}$ measurements.

749

750 **References**

751

- 752 Agrawal, D. P.: The Indus Civilization: an interdisciplinary perspective, Aryan Books
753 International, New Delhi, India, 2007.
- 754 Ahmad, N., Mohammad, A., and Khan, S. T.: Country Report on Water resources of Pakistan,
755 in South Asia Water Balance Workshop. Hansen Institute for World Peace, San Diego,
756 California, USA, 30 April – 2 May 2001, 2001.
- 757 Bar-Matthews, M., and Ayalon, A.: Mid-Holocene climate variations revealed by high-
758 resolution speleothem records from Soreq Cave, Israel and their correlation with cultural
759 changes, *The Holocene*, 21, 163-171, 2011.
- 760 Bar-Matthews, M., Ayalon, A., Gilmour, M., Matthews, A., and Hawkesworth, C. J.: Sea–land
761 oxygen isotopic relationships from planktonic foraminifera and speleothems in the
762 Eastern Mediterranean region and their implication for paleorainfall during interglacial
763 intervals, *Geochimica et Cosmochimica Acta*, 67, 3181-3199, 2003.
- 764 Bé, A. W., and Hutson, W. H.: Ecology of planktonic foraminifera and biogeographic patterns
765 of life and fossil assemblages in the Indian Ocean, *Micropaleontology*, 369-414, 1977.
- 766 Bemis, B. E., Spero, H. J., Bijma, J., and Lea, D. W.: Reevaluation of the oxygen isotopic
767 composition of planktonic foraminifera: Experimental results and revised
768 paleotemperature equations. *Paleoceanography*, 13, 150-160, 1998.
- 769 Berkelhammer, M., Sinha, A., Stott, L., Cheng, H., Pausata, F. S., and Yoshimura, K.: An
770 abrupt shift in the Indian monsoon 4000 years ago, *Geophys. Monogr. Ser.*, 198, 2012.
- 771 Billups, K., Ravelo, A. C., Zachos, J. C., and Norris, R. D.: Link between oceanic heat transport,
772 thermohaline circulation, and the Intertropical Convergence Zone in the early Pliocene
773 Atlantic, *Geology*, 27, 319-322, 1999.
- 774 Blaauw, M., and Christen, J. A.: Flexible paleoclimate age–depth models using an
775 autoregressive gamma process, *Bayesian analysis*, 6, 457-474, 2011.
- 776 Cheng, H., Sinha, A., Verheyden, S., Nader, F. H., Li, X. L., Zhang, P. Z., Yin, J. J., Yi, L., Peng., Y.
777 B., Rao, Z. G., Ning, Y. F., and Edwards, R. L.: The climate variability in northern Levant
778 over the past 20,000 years, *Geophysical Research Letters*, 42, 8641-8650, 2015.
- 779 Cannariato, K.G., and Ravelo, A.C.: Pliocene-Pleistocene evolution of eastern tropical Pacific
780 surface water circulation and thermocline depth. *Paleoceanography*, 12, 805-820, doi:
781 10.1029/97PA02514, 1997.
- 782 Cayre, O., and Bassinot, F.: Oxygen isotope composition of planktonic foraminiferal shells
783 over the Indian Ocean: calibration to modern oceanographic data. *Mineral Mag*, 62, 288-
784 289, 1998.
- 785 Curry, W. B., Ostermann, D. R., Guptha, M. V. S., and Ittekkot, V.: Foraminiferal production
786 and monsoonal upwelling in the Arabian Sea: evidence from sediment traps, *Geological*
787 *Society, London, Special Publications*, 64, 93-106, 1992.



- 788 Cullen, H. M., deMenocal, P. B., Hemming, S., Hemming, G., Brown, F. H., Guilderson, T., and
789 Sirocko, F.: Climate change and the collapse of the Akkadian empire: Evidence from the
790 deep sea, *Geology*, 28, 379-382, 2000.
- 791 Dahl, K. A., and Oppo, D. W.: Sea surface temperature pattern reconstructions in the
792 Arabian Sea, *Paleoceanography*, 21, 2006.
- 793 Deotare, B. C., Kajale, M. D., Rajaguru, S. N., Kusumgar, S., Jull, A. J. T., and Donahue, J. D.:
794 Palaeoenvironmental history of Bap-Malar and Kanod playas of western Rajasthan, Thar
795 desert, *Journal of Earth System Science*, 113, 403-425, 2004.
- 796 Dimri, A. P.: Surface and upper air fields during extreme winter precipitation over the
797 western Himalayas, *Pure and Applied Geophysics*, 163, 1679-1698, 2006.
- 798 Dimri, A. P., and Dash, S. K.: Wintertime climatic trends in the western Himalayas. *Climatic*
799 *Change*, 111, 775-800, 2012.
- 800 Dixit, Y., Hodell, D. A., and Petrie, C. A.: Abrupt weakening of the summer monsoon in
801 northwest India ~4100 yr ago, *Geology*, 42, 339-342, 2014.
- 802 Dixit, Y., Hodell, D. A., Giesche, A., Tandon, S. K., Gázquez, F., Saini, H. S., Skinner, L. C.,
803 Mujtaba, S. A. I., Pawar, V., Singh, R.N., and Petrie, C. A.: Intensified summer monsoon
804 and the urbanization of Indus Civilization in northwest India, *Scientific reports*, 8, 4225,
805 2018.
- 806 Dooze-Rolinski, H., Rogalla, U., Scheeder, G., Lückge, A., and Rad, U.: High-resolution
807 temperature and evaporation changes during the late Holocene in the northeastern
808 Arabian Sea, *Paleoceanography and Paleoclimatology*, 16, 358-367, 2001.
- 809 Duplessy, J. C., Labeyrie, L., Arnold, M., Paterne, M., Duprat, J., and van Weering, T. C.:
810 Changes in surface salinity of the North Atlantic Ocean during the last deglaciation.
811 *Nature*, 358, 485, 1992.
- 812 Enzel, Y., Ely, L. L., Mishra, S., Ramesh, R., Amit, R., Lazar, B., Rajaguru, S.N., Baker, V. R., and
813 Sandler, A.: High-resolution Holocene environmental changes in the Thar Desert,
814 northwestern India, *Science*, 284, 125-128, 1999.
- 815 Farmer, E. C., Kaplan, A., de Menocal, P. B., and Lynch-Stieglitz, J.: Corroborating ecological
816 depth preferences of planktonic foraminifera in the tropical Atlantic with the stable
817 oxygen isotope ratios of core top specimens, *Paleoceanography*, 22, 2007.
- 818 Finné, M., Holmgren, K., Sundqvist, H. S., Weiberg, E., and Lindblom, M.: Climate in the
819 eastern Mediterranean, and adjacent regions, during the past 6000 years—A review,
820 *Journal of Archaeological Science*, 38, 3153-3173, 2011.
- 821 Fleitmann, D., Burns, S. J., Mudelsee, M., Neff, U., Kramers, J., Mangini, A., and Matter, A.:
822 Holocene forcing of the Indian monsoon recorded in a stalagmite from southern Oman,
823 *Science*, 300, 1737-1739, 2003.
- 824 Fleitmann, D., Burns, S. J., Mangini, A., Mudelsee, M., Kramers, J., Villa, I., Neff, U., Al-
825 Subbary, A. A., Buettner, A., Hippler, D., and Matter, A.: Holocene ITCZ and Indian
826 monsoon dynamics recorded in stalagmites from Oman and Yemen (Socotra), *Quaternary*
827 *Science Reviews*, 26, 170-188, 2007.
- 828 Gadgil, S.: The Indian monsoon and its variability, *Annual Review of Earth and Planetary*
829 *Sciences*, 31, 429-467, 2003.
- 830 Giosan, L., Clift, P. D., Macklin, M. G., Fuller, D. Q., Constantinescu, S., Durcan, J. A., Stevens,
831 T., Duller, G. A. T., Tabrez, A. R., Gangal, K., Adhikari, R., Alizai, A., Filip, F., VanLaningham,
832 S., and Syvitski, J. P. M.: Fluvial landscapes of the Harappan civilization, *Proceedings of*
833 *the National Academy of Sciences*, 109, E1688-E1694, 2012.



- 834 Giosan, L., Orsi, W. D., Coolen, M., Wuchter, C., Dunlea, A. G., Thirumalai, K., Munoz, S. E.,
835 Clift, P. D., Donnelly, J. P., Galy, V., and Fuller, D. Q.: Neoglacial Climate Anomalies and
836 the Harappan Metamorphosis, *Clim. Past Discuss.*, doi:10.5194/cp-2018-37, in review,
837 2018.
- 838 Green, A. S., Bates, J., Acabado, S., Coutros, P., Glover, J., Miller, N., Sharratt, N., and Petrie,
839 C.A.: How to Last a Millennium; Or a Global Perspective on the Long-Term Dynamics of
840 Human Sustainability, in preparation for *Nature Sustainability*.
- 841 Green, A. S., and Petrie, C. A.: Landscapes of Urbanization and De-Urbanization: A Large-
842 Scale Approach to Investigating the Indus Civilization's Settlement Distributions in
843 Northwest India, *Journal of Field Archaeology*, 1-16, 2018.
- 844 Gupta, A. K., Anderson, D. M., and Overpeck, J. T.: Abrupt changes in the Asian southwest
845 monsoon during the Holocene and their links to the North Atlantic Ocean. *Nature*, 421,
846 354, 2003.
- 847 Hastenrath, S., and Lamb, P. J.: Climatic atlas of the Indian Ocean. Part II: The oceanic heat
848 budget, Wisconsin University Press, Madison, Wisconsin, USA, 93, 17, 1979.
- 849 Hatwar, H. R., Yadav, B. P., and Rao, Y. R.: Prediction of western disturbances and associated
850 weather over Western Himalayas, *Current science*, 913-920, 2005.
- 851 Hemleben, C., Spindler, M., and Anderson, O. R.: Modern planktonic foraminifera. Springer
852 Science and Business Media, 2012.
- 853 Joseph, S., and Freeland, H. J.: Salinity variability in the Arabian Sea. *Geophysical research*
854 *letters*, 32, 2005.
- 855 Karim, A., and Veizer, J.: Water balance of the Indus River Basin and moisture source in the
856 Karakoram and western Himalayas: Implications from hydrogen and oxygen isotopes in
857 river water, *Journal of Geophysical Research: Atmospheres*, 107, ACH-9, 2002.
- 858 Kathayat, G., Cheng, H., Sinha, A., Yi, L., Li, X., Zhang, H., Li, H., Ning, Y., and Edwards, R. L.:
859 The Indian monsoon variability and civilization changes in the Indian subcontinent,
860 *Science advances*, 3, e1701296, 2017.
- 861 Kim, S. T., and O'Neil, J. R.: Equilibrium and nonequilibrium oxygen isotope effects in
862 synthetic carbonates, *Geochimica et Cosmochimica Acta*, 61, 3461-3475, 1997.
- 863 Lemcke, G., and Sturm, M.: $\delta^{18}\text{O}$ and trace element measurements as proxy for the
864 reconstruction of climate changes at Lake Van (Turkey): Preliminary results, in *Third*
865 *millennium BC climate change and Old World collapse*, Springer, Berlin, Heidelberg,
866 Germany, 653-678, 1997.
- 867 Lynch-Stieglitz, J.: Tracers of past ocean circulation, in: *Treatise on geochemistry*, 6,
868 Elderfield, H., Holland, H. D., and Turekian, K. K. (Eds), Elsevier, 433-451, 2006.
- 869 Madella, M., and Fuller, D. Q.: Palaeoecology and the Harappan Civilisation of South Asia: a
870 reconsideration, *Quaternary Science Reviews*, 25, 1283-1301, 2006.
- 871 Maslin, M. A., Shackleton, N. J., and Pflaumann, U.: Surface water temperature, salinity, and
872 density changes in the northeast Atlantic during the last 45,000 years: Heinrich events,
873 deep water formation, and climatic rebounds, *Paleoceanography*, 10, 527-544, 1995.
- 874 Mayewski, P. A., Rohling, E. E., Stager, J. C., Karlén, W., Maasch, K. A., Meeker, L. D.,
875 Meyerson, E. A., Gasse, F., van Kreveld, S., Holmgren, K., Lee-Thorp, J., Rosqvist, G., Rack,
876 F., Staubwasser, M., Schneider, R.R., and Steig, E.J.: Holocene climate variability,
877 *Quaternary research*, 62, 243-255, 2004.
- 878 Menzel, P., Gaye, B., Mishra, P. K., Anoop, A., Basavaiah, N., Marwan, N., Plessen, B., Prasad,
879 S., Riedel, N., Stebich, M., and Wiesner, M. G.: Linking Holocene drying trends from Lonar



- 880 Lake in monsoonal central India to North Atlantic cooling events, *Palaeogeography,*
881 *palaeoclimatology, palaeoecology*, 410, 164-178, 2014.
- 882 Nakamura, A., Yokoyama, Y., Maemoku, H., Yagi, H., Okamura, M., Matsuoka, H., Miyake,
883 N., Osada, T., Adhikari, D. P., Dangol, V., Ikehara, M., Miyairi, Y., and Matsuzaki, H.: Weak
884 monsoon event at 4.2 ka recorded in sediment from Lake Rara, Himalayas, *Quaternary*
885 *International*, 397, 349-359, 2016.
- 886 Norris, R. D.: Planktonic foraminifer biostratigraphy: eastern equatorial Atlantic, in:
887 *Proceedings of the Ocean Drilling Program: Scientific results*, 159, 445-479, 1998.
- 888 Overpeck, J., Anderson, D., Trumbore, S., and Prell, W.: The southwest Indian Monsoon over
889 the last 18000 years. *Climate Dynamics*, 12, 213-225, 1996.
- 890 Petrie, C. A., and Bates, J.: 'Multi-cropping', Intercropping and Adaptation to Variable
891 Environments in Indus South Asia. *Journal of World Prehistory*, 30, 81-130, 2017.
- 892 Petrie, C. A., Bates, J., Higham, T., and Singh, R. N.: Feeding ancient cities in South Asia:
893 dating the adoption of rice, millet and tropical pulses in the Indus civilisation. *Antiquity*,
894 90, 1489-1504, 2016.
- 895 Petrie, C. A., Singh, R. N., Bates, J., Dixit, Y., French, C. A., Hodell, D. A., Pandey, A. K., Parikh,
896 D., Pawar, V., Redhouse, D. I., and Singh, D. P.: Adaptation to variable environments,
897 resilience to climate change: Investigating land, water and settlement in Indus Northwest
898 India, *Current Anthropology*, 58, 2017.
- 899 Phadtare, N. R.: Sharp decrease in summer monsoon strength 4000–3500 cal yr BP in the
900 Central Higher Himalaya of India based on pollen evidence from alpine peat, *Quaternary*
901 *Research*, 53, 122-129, 2000.
- 902 Pokharia, A. K., Agnihotri, R., Sharma, S., Bajpai, S., Nath, J., Kumaran, R. N., and Negi, B. C.:
903 Altered cropping pattern and cultural continuation with declined prosperity following
904 abrupt and extreme arid event at ~4,200 yrs BP: Evidence from an Indus archaeological
905 site Khirsara, Gujarat, western India, *PLoS one*, 12, 2017.
- 906 Ponton, C., Giosan, L., Eglinton, T. I., Fuller, D. Q., Johnson, J. E., Kumar, P., and Collett, T. S.:
907 Holocene aridification of India, *Geophysical Research Letters*, 39, 2012.
- 908 Possehl, G. L.: The transformation of the Indus civilization, *Journal of World Prehistory*, 11,
909 425-472, 1997.
- 910 Possehl, G. L.: *The Indus Civilization: a Contemporary Perspective*. Rowman Altamira, 2002.
- 911 Possehl, G. L.: *The Indus Civilization: an introduction to environment, subsistence, and*
912 *cultural history*. *Indus ethnobiology*, 1-20, 2003.
- 913 Prasad, S., and Enzel, Y.: Holocene paleoclimates of India. *Quaternary Research*, 66, 442-
914 453, 2006.
- 915 Ramasastri, K.S.: Snow melt modeling studies in India, in: *The Himalayan Environment*, S.K.
916 Dash and J. Bahadur (Eds.), New Age International, 59–70, 1999.
- 917 Rangachary, N., and Bandyopadhyay, B. K.: An analysis of the synoptic weather pattern
918 associated with extensive avalanching in Western Himalaya, *Int. Assoc. of Hydrol. Sci.*
919 *Publ*, 162, 311-316, 1987.
- 920 Rao, Y.P.: The Climate of the Indian Sub-Continent, in: *World Survey of Climatology*, 9,
921 *Climates of Southern and Western Asia*, Elsevier, Amsterdam, Netherlands, 67-182, 1981.
- 922 Ravelo, A.C., and Shackleton, N.J.: Evidence for surface-water circulation changes at Site 851
923 in the eastern Tropical Pacific Ocean, in: *Proceedings of the Ocean Drilling Program,*
924 *Scientific Results*, College Station, TX (Ocean Drilling Program), Pisias, N. G.; Mayer, L. A.;
925 Janecek, T. R.; Palmer-Julson, A.; van Andel, T. H. (Eds.), 138, 503-514, doi:
926 10.2973/odp.proc.sr.138.126, 1995.



- 927 Reimer, P. J., Bard, E., Bayliss, A., Beck, J. W., Blackwell, P. G., Ramsey, C. B., Buck, C. E.,
928 Cheng, H., Edwards, R. L., Friedrich, M., Grootes, P. M., Guilderson, T. P., Hafliðason, H.,
929 Hajdas, I., Hatté, C., Heaton, T. J., Hoffmann, D. L., Hogg, A. G., Hughen, K. A., Kaiser, K. F.,
930 Kromer, B., Manning, St.W., Niu, M., Reimer, R. W., Richards, D. A., Scott, E. M., Southon,
931 J. R., Staff, R. A., Turney, C. S. M., and van der Plicht, J.: IntCal13 and Marine13
932 radiocarbon age calibration curves 0–50,000 years cal BP, *Radiocarbon*, 55, 1869-1887,
933 2013.
- 934 Rohling, E. J.: Paleosalinity: confidence limits and future applications, *Marine Geology*, 163,
935 1-11, 2000.
- 936 Schulz, H., von Rad, U., and Ittekkot, V.: Planktic foraminifera, particle flux and oceanic
937 productivity off Pakistan, NE Arabian Sea: modern analogues and application to the
938 palaeoclimatic record, Geological Society, London, Special Publications, 195, 499-516,
939 2002.
- 940 Shackleton, N. J.: Attainment of isotopic equilibrium between ocean water and the
941 benthonic foraminifera genus *Uvigerina*: isotopic changes in the ocean during the last
942 glacial, *Colloques Internationaux du C.N.R.S.*, 1974.
- 943 Shenoj, S. S. C., Shankar, D., and Shetye, S. R.: Differences in heat budgets of the near-
944 surface Arabian Sea and Bay of Bengal: Implications for the summer monsoon, *Journal of*
945 *Geophysical Research: Oceans*, 107, 5-1, 2002.
- 946 Singh, G., Wasson, R. J., and Agrawal, D. P.: Vegetational and seasonal climatic changes since
947 the last full glacial in the Thar Desert, northwestern India, *Review of Palaeobotany and*
948 *Palynology*, 64, 351-358, 1990.
- 949 Sinha, R., Smykatz-Kloss, W., Stüben, D., Harrison, S. P., Berner, Z., and Kramar, U.: Late
950 Quaternary palaeoclimatic reconstruction from the lacustrine sediments of the Sambhar
951 playa core, Thar Desert margin, India, *Palaeogeography, Palaeoclimatology,*
952 *Palaeoecology*, 233, 252-270, 2006.
- 953 Sirocko, F.: Deep-sea sediments of the Arabian Sea: A paleoclimatic record of the
954 southwest-Asian summer monsoon, *Geologische Rundschau*, 80, 557-566, 1991.
- 955 Sonderegger, D. L., Wang, H., Clements, W. H., and Noon, B. R.: Using SiZer to detect
956 thresholds in ecological data, *Frontiers in Ecology and the Environment*, 7, 190-195,
957 2009.
- 958 Staubwasser, M., Sirocko, F., Grootes, P. M., and Erlenkeuser, H.: South Asian monsoon
959 climate change and radiocarbon in the Arabian Sea during early and middle Holocene,
960 *Paleoceanography and Paleoclimatology*, 17, 2002.
- 961 Staubwasser, M., Sirocko, F., Grootes, P. M., and Segl, M.: Climate change at the 4.2 ka BP
962 termination of the Indus valley civilization and Holocene south Asian monsoon variability,
963 *Geophysical Research Letters*, 30, 2003.
- 964 Staubwasser, M., and Weiss, H.: Holocene climate and cultural evolution in late prehistoric–
965 early historic West Asia, *Quaternary Research*, 66, 372-387, 2006.
- 966 Staubwasser, M.: Late Holocene Drought Pattern Over West Asia. *Climates, Landscapes, and*
967 *Civilizations*, 89-96, 2012.
- 968 Steinke, S., Mohtadi, M., Groeneveld, J., Lin, L. C., Löwemark, L., Chen, M. T., and Rendle-
969 Bühring, R.: Reconstructing the southern South China Sea upper water column structure
970 since the Last Glacial Maximum: Implications for the East Asian winter monsoon
971 development, *Paleoceanography and Paleoclimatology*, 25, 2010.



- 972 Steph, S., Regenberg, M., Tiedemann, R., Mulitza, S., and Nürnberg, D.: Stable isotopes of
973 planktonic foraminifera from tropical Atlantic/Caribbean core-tops: Implications for
974 reconstructing upper ocean stratification. *Marine Micropaleontology*, 71, 1-19, 2009.
- 975 Tian, J., Wang, P., Chen, R., and Cheng, X.: Quaternary upper ocean thermal gradient
976 variations in the South China Sea: Implications for east Asian monsoon climate,
977 *Paleoceanography*, 20, 2005.
- 978 Von Rad, U., Schulz, H., Khan, A. A., Ansari, M., Berner, U., Čepek, P., Cowie, G., Dietrich, P.,
979 Erlenkeuser, H., Geyh, M., Jennerjahn, T., Lückge, A., Marchig, V., Riech, V., Rösch, H.,
980 Schäfer, P., Schulte, S., Sirocko, F., and Tahir, M.: Sampling the oxygen minimum zone off
981 Pakistan: glacial-interglacial variations of anoxia and productivity (preliminary results,
982 SONNE 90 cruise), *Marine Geology*, 125, 7-19, 1995.
- 983 Von Rad, U.: Physical oceanography during SONNE cruise SO90, PANGAEA,
984 doi:10.1594/PANGAEA.805802, 2013.
- 985 Walker, M. J., Berkelhammer, M., Björck, S., Cwynar, L. C., Fisher, D. A., Long, A. J., Lowe, J.
986 J., Newnham, R. M., Rasmussen, S. O., and Weiss, H.: Formal subdivision of the Holocene
987 Series/Epoch: a Discussion Paper by a Working Group of INTIMATE (Integration of ice-
988 core, marine and terrestrial records) and the Subcommittee on Quaternary Stratigraphy
989 (International Commission on Stratigraphy), *Journal of Quaternary Science*, 27, 649-659,
990 2012.
- 991 Wang, L., Sarnthein, M., Duplessy, J. C., Erlenkeuser, H., Jung, S., and Pflaumann, U.: Paleo
992 sea surface salinities in the low-latitude Atlantic: The $\delta^{18}\text{O}$ record of *Globigerinoides*
993 *ruber* (white), *Paleoceanography*, 10, 749-761, 1995.
- 994 Wanner, H., Beer, J., Bütikofer, J., Crowley, T. J., Cubasch, U., Flückiger, J., Goosse, H.,
995 Grosjean, M., Joos, F., Kaplan, J. O., Küttel, M., Müller, S. A., Prentice, C., Solomina, O.,
996 Stocker, T. F., Tarasov, P., Wagner, M., and Widmann, M.: Mid-to Late Holocene climate
997 change: an overview, *Quaternary Science Reviews*, 27, 1791-1828, 2008.
- 998 Weber, S.: Seeds of urbanism: palaeoethnobotany and the Indus Civilization, *Antiquity*, 73,
999 813-826, 1999.
- 1000 Weber, S. A.: Archaeobotany at Harappa: indications for change, *Indus ethnobiology: new*
1001 *perspectives from the field*, 175-198, 2003.
- 1002 Weber, S. A., Barela, T., and Lehman, H.: Ecological continuity: An explanation for
1003 agricultural diversity in the Indus Civilization and beyond, *Man and Environment*, 35, 62-
1004 75, 2010.
- 1005 Weiss, H.: Global megadrought, societal collapse and resilience at 4.2-3.9 ka BP across the
1006 Mediterranean and West Asia, *Clim. Chang. Cult. Evol*, PAGES Mag, 24, 62, 2016.
- 1007 Wheeler, M.: *The Indus Civilization*, Cambridge University Press, Great Britain, 1968.
- 1008 Wick, L., Lemcke, G., and Sturm, M.: Evidence of Lateglacial and Holocene climatic change
1009 and human impact in eastern Anatolia: high-resolution pollen, charcoal, isotopic and
1010 geochemical records from the laminated sediments of Lake Van, Turkey. *The Holocene*,
1011 13, 665-675, 2003.
- 1012 Wright, R. P.: *The ancient Indus: urbanism, economy, and society*, Cambridge University
1013 Press, Great Britain, 107, 2010.
- 1014 Yadav, R. K., Kumar, K. R., and Rajeevan, M.: Characteristic features of winter precipitation
1015 and its variability over northwest India. *J. Earth Syst. Sci.*, 121, 611-623, 2012.
- 1016 Yu, W., Yang, Y. C., Savitsky, A., Alford, D., Brown, C., Wescoat, J., Debowicz, D., and
1017 Robinson, S.: *The Indus basin of Pakistan: The impacts of climate risks on water and*
1018 *agriculture*, The World Bank, 2013.



- 1019 Zaric, S.: Planktic foraminiferal flux of sediment trap EAST-86/90_trap, PANGAEA, doi:
1020 10.1594/PANGAEA.264508, 2005.
- 1021 Zweng, M. M., Reagan, J. R., Antonov, J. I., Locarnini, R. A., Mishonov, A. V., Boyer, T. P.,
1022 Garcia, H. E., Baranova, O. K., Johnson, D. R., Seidov, D., and Biddle, M. M.: World Ocean
1023 Atlas 2013, Volume 2: Salinity. Levitus, S. (Ed.), Mishonov, A. (Technical Ed.), NOAA Atlas
1024 NESDIS 74, 39, 2013.